The Dissertation Committee for Zeyu Yan
Certifies that this is the approved version of the following dissertation:

Numerical Optimal Control of a Wind Turbine System

Committee:

Dongmei Chen, Supervisor

Eric P. Fahrenthold

Neal A. Hall

Wei Li

Carolyn C. Seepersad

Numerical Optimal Control of a Wind Turbine System

by

Zeyu Yan, B. E.; M. S. E.

Dissertation

Presented to the Faculty of the Graduate School of

The University of Texas at Austin

in Partial Fulfillment

of the Requirements

for the Degree of

Doctor of Philosophy

The University of Texas at Austin

August 2015

Acknowledgements

First of all, I would like to express my earnest gratitude to my advisor, Dr. Dongmei Chen. She gave me a lot of help on my research and career plan. She is always ready to help me when I met problems, no matter how busy she is.

Second, I would like to thank all of my committee members: Dr. Fahrenthold, Dr. Hall, Dr. Li and Dr. Seepersad. Thank you so much for being my committee members and your helpful advice.

Third, I would like to thank all of my research group members. We are like a big family and I have learned a lot from all you guys. You are really talented guys and we will be brothers forever.

Finally, I would like to thank my parents, my best friends: Changyi Jiang, Siyuan Huang, Ziyi Jiang and etc. Without your support, I would not be able to get where I am today. Thank you very much and I love you all!

This work was supported by National Science Foundation (NSF)-Control Systems Program CAREER Award CMMI-1056020 and the Department of Mechanical Engineering at the University of Texas at Austin.

Numerical Optimal Control of a Wind Turbine System

Zeyu Yan, Ph. D.

The University of Texas at Austin, 2015

Supervisor: Dongmei Chen

With the development of wind turbine technology and the need for maximizing wind energy harvesting, more wind turbines operate in the partial load region. Among many control algorithms developed for this region, controllers based on feedback of the global maximum power coefficient have been widely used. These control schemes offer good performance with simple implementations, but they may not be suited for wind turbines with limited rotor speed ranges. In such cases, the controller is challenged because the main feature ---the global maximum power coefficient--- is not achievable due to the turbine speed constraint. It is necessary to develop a controller to seek the achievable maximum power coefficient that leads to optimal wind energy capture. In this dissertation, the development of an optimal control framework to maximize wind energy capture for wind turbines with constrained turbine speed is first presented. Numerical optimal control techniques are applied to search for the achievable maximum power coefficient, with proposed modifications to make this task more computationally feasible.

Mitigating the turbine generator torque variation, thus reducing the fatigue loading on turbine generator shaft, is also important for the partial load region operation. Including this aspect in the optimal control is then discussed. Furthermore, an approach of incorporating time-varying weightings into developing the optimal controller is introduced

to seek further improvement on turbine generator torque variation reduction, thus fatigue reduction.

In addition, the power generated by the wind turbine varies due to variation in the wind speed. Depending on the load demand and the wind speed, the wind turbine's operation switches between two modes: a multi-input-single-output (MISO) mode and a single-input-single-output (SISO) mode. Due to the wind turbine changes its dynamic behavior during the switching process, applying the traditional control methods to each corresponding mode may not be capable of maximizing the overall wind energy capture throughout the entire turbine's operation. Therefore, the development of an optimal control framework to maximize the overall wind energy capture for a switched wind turbine system is subsequently presented.

Table of Contents

List of Tables

List of Figures

Chapter 1: *Introduction*

BACKGROUND

Wind energy, considered as one of the renewable resources, is becoming more important in displacement of the fossil fuel to provide electric energy. It is a widely distributed and plentiful resource. The total amount of economically extractable power available from the wind is considerably more than present human power use from all other sources. Besides, the wind energy is clean and won't generate greenhouse effect. Therefore, utilization of wind energy has rapidly increased in recent years. Figure 1 shows the U.S. energy chart of 2013 [1]. From Fig. 1, it can be seen that the source of 13% of the total energy consumption is renewable energy and a portion of 2.3% is contributed by wind energy.

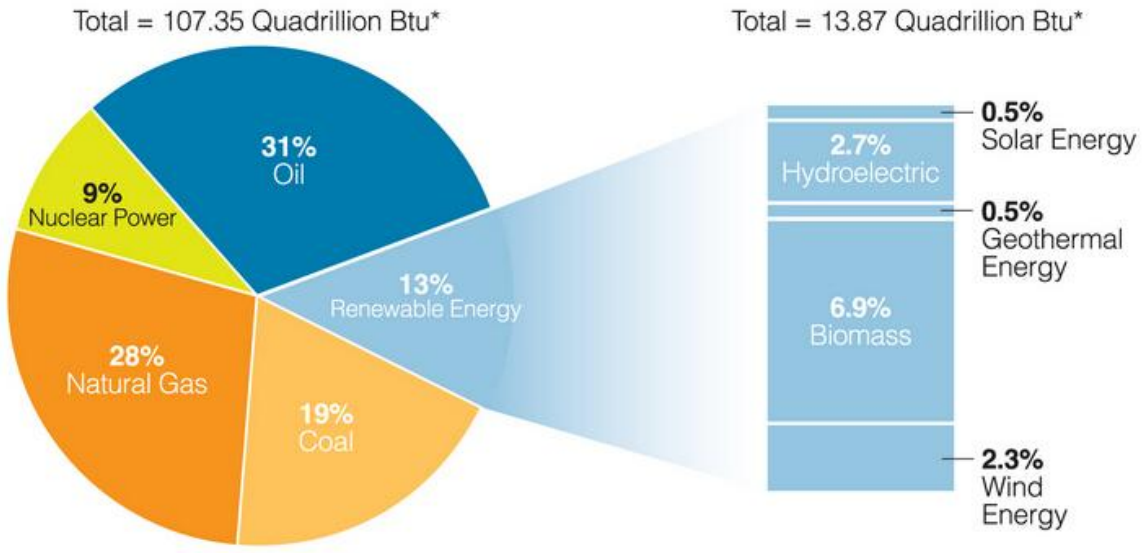

Figure 1: U.S. energy chart 2013 [1].

Wind energy has played an important role in supporting the electrical power grid. According to the U.S. Department of Energy, wind has been the fastest growing source of electricity generation in the world through the 1990s [2]. In 2006, President Bush emphasized the nation's need for greater energy efficiency and a more diversified energy portfolio. This led to a collaborative effort to explore a modeled energy scenario in which wind provides 20% of U.S. electricity by 2030. With great technology advancements, traditional windmills have been replaced by specially designed wind turbines, which enhance the productivity of electricity. Figs. 2 and 3 show the global annual and cumulative installed wind capacity through the years 1996 to 2013 [3]. From Figs. 2 and 3, it can be seen that the global annual and cumulative installed wind capacity are basically keep increasing through the years 1996 to 2013.

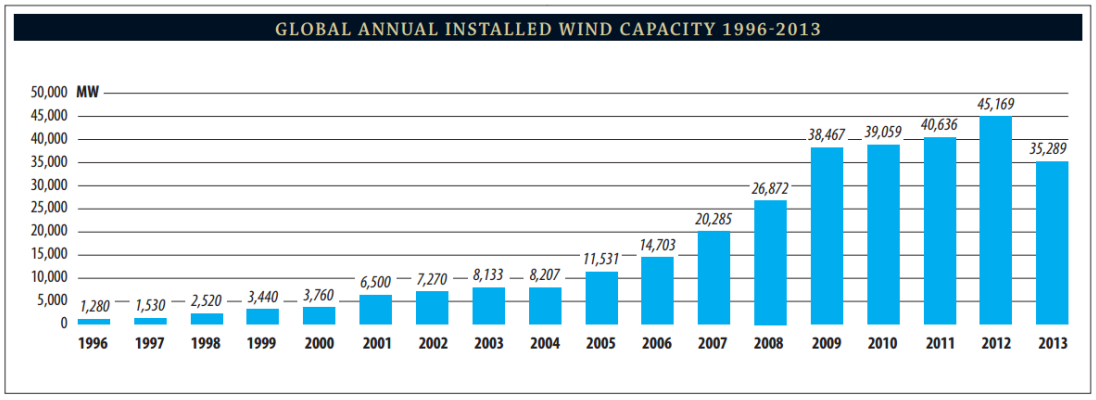

Figure 2: Global annual installed wind capacity 1996-2013 [3].

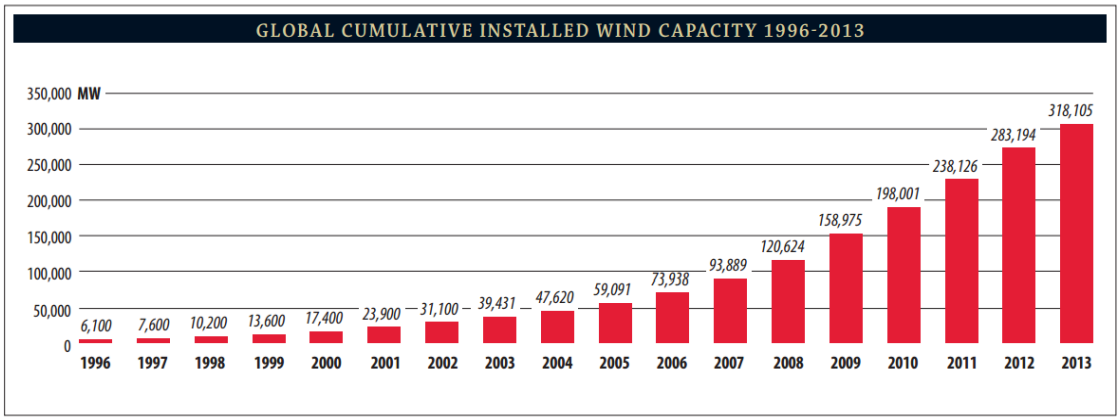

Figure 3: Global cumulative installed wind capacity 1996-2013 [3].

In the near future, wind energy will be the most cost effective source of electrical power. In fact, a good case can be made for saying that it already has achieved this status. The major technology developments enabling wind power commercialization have already been made. There will be infinite refinements and improvements, of course. Furthermore, political and economic requirements have changed dramatically because global environmental problems can no longer be ignored. International environmental treaties, such as the Kyoto Protocol, establish legally binding commitments for the reduction of greenhouse gas concentrations in the atmosphere and industrialized countries agreed to reduce their collective GHG (greenhouse gas) emissions. International, standardized applications for renewable energies, regardless of national regulations or climate conditions, are more and more likely to be put into place. The wind energy industry's future looks optimistic.

As an important device that converts the kinetic energy from the wind into mechanical energy, maximizing the efficiency of wind turbine plays an important role in the development of the wind power. Especially in wind farms where hundreds of wind

turbines are installed, the efficiency improvement of an individual wind turbine could result in a significant energy gain for the entire wind farm and this will make the wind energy more economically viable. Therefore, the main goal of our research is to improve wind turbine's operation efficiency.

TYPES OF WIND TURBINES

Wind turbine is a device that converts kinetic energy from the wind into electrical energy and a wind farm is a group of wind turbines in the same location used to produce electric power. Wind turbines can be separated into two basic types determined by which way the turbine spins. Horizontal axis wind turbines, also shortened to HAWTs, are the common style when most of us think about a wind turbine. There are also vertical axis wind turbines, shortened as VAWTs, have the main rotor shaft arranged vertically. Figure 4 illustrates these two basic types of wind turbines [4]. Basically most HAWTs have an average increased efficiency from a common VAWT. This is mainly because of the additional drag that the VAWTs have as their blades rotate into the wind. Due to this main reason, HAWTs are more common while VAWTs are less frequently used in wind farms. We will focus on the control methodology of a HAWT model in our research.

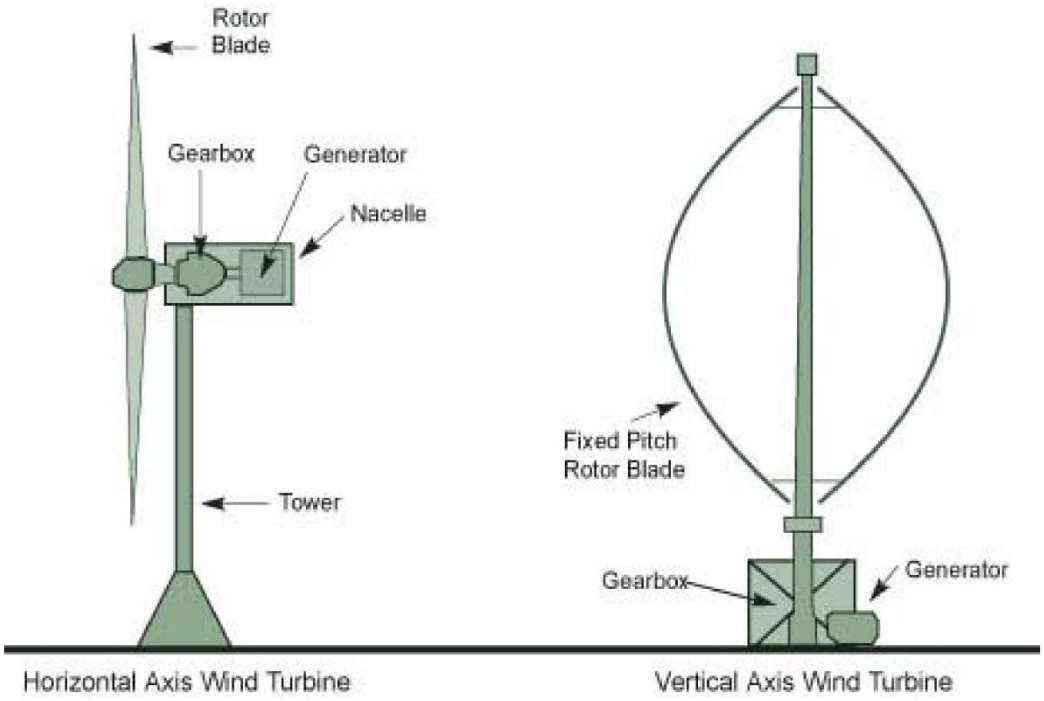

Figure 4: Different types of wind turbines [4].

TURBINE STRUCTURE

Figure 5 shows the detailed structure of a typical HAWT. It is made up of the following components [5]:

1. Tower and foundation

   In order to guarantee the stability of a wind turbine a pile or flat foundation is used, depending on the consistency of the underlying ground.

   The tower construction doesn't just carry the weight of the nacelle and the rotor blades, but must also absorb the huge static loads caused by the varying power of the wind. Generally, a tubular construction of concrete or steel is used. An alternative to this is the lattice tower form.

2. Rotor and blades

The rotor is the component, which, with the help of the blades, converts the energy from the wind into rotary mechanical movement.

Currently, the three-blade, horizontal axis rotor dominates. The rotor blades are mainly made of glass-fiber or carbon-fiber reinforced plastics (GRP, CFRP). The blade profile is similar to that of an airplane wing. They use the same principle of lift: on the lower side of the wing the passing air generates higher pressure, while the upper side generates a pull. These forces cause the rotor to move forwards, i.e. to rotate. The pitch refers to turning the angle of attack of the blades into or out of the wind.

3. Nacelle with drivetrain

The nacelle holds all the turbine machinery. Because it must be able to rotate to follow the wind direction, it is connected to the tower via bearings. The build-up of the nacelle shows how the manufacturer has decided to position the drive train components (rotor shaft with bearings, transmission, generator, coupling and brake) above this machine bearing.

a) Gearbox

The gearbox converts the rotor motion into the proper range, which the generator requires.

b) Generator

The generator is the component, which converts mechanical movement into electrical energy. Table 1 shows the common generator types for modern wind turbines [6].

Type	Generator Type	Rotor Speed (Allowable variation from grid synchronous speed)
A	Squirrel Cage Induction Generator	+1%
B	Wound Rotor Induction Generator	+10%
C	Doubly-Fed Induction Generator	-40% to +30%
D	Synchronous Generator	Independent

Table 1: Different types of turbine generators and their speed range [6].

Induction generators are often used in wind turbines and some micro hydro installations due to their ability to produce useful power at varying rotor speeds. Induction generators are mechanically and electrically simpler than other generator types. They are also more rugged, requiring no brushes or commutators. Induction generators are particularly suitable for wind generating stations as in this case speed is always a variable factor. Unlike synchronous motors, induction generators are load-dependent and cannot be used alone for grid frequency control.

The synchronous generators are only used for a small number of small wind turbines, mainly for stand-alone systems.

c) Coupling and brake

Because of the enormous torque, the coupling between the main shaft and the transmission is a rigid one. The type of brake depends on the control mechanism for the blades. There are two main types of turbine brakes: electrical and mechanical brakes. Electrical braking is useful if the kinetic load on the generator is suddenly reduced or is too small to keep the turbine speed within its allowed limit. On the other hand, the mechanical braking is a secondary and usually applied only

after blade furling and electromagnetic braking have reduced the turbine speed generally 1 or 2 rotor RPM, as the mechanical brakes can create a fire inside the nacelle if used to stop the turbine from full speed.

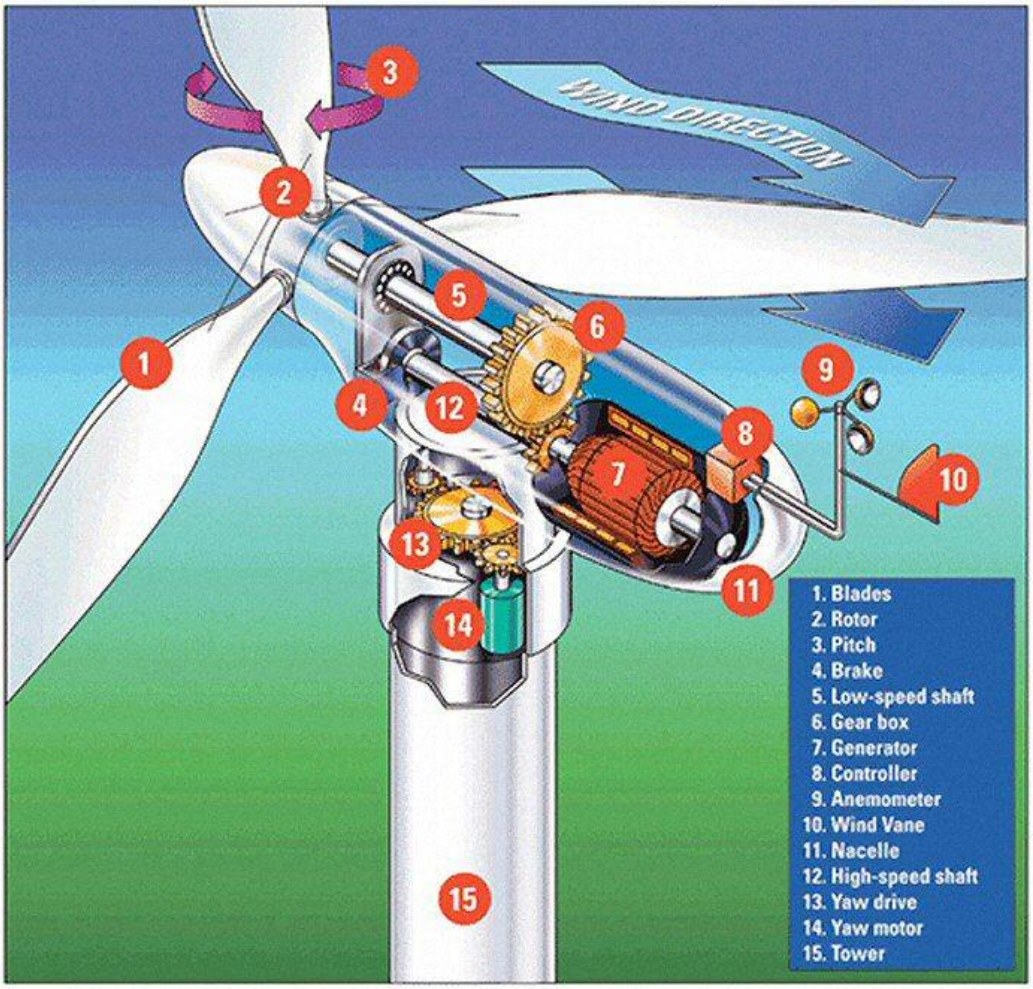

Figure 5: Typical structure of a HWAT [5].

REGIONS OF OPERATION

There are four operation regions for a wind turbine system, which are defined in Fig. 6 [7]. In Region 1, which is also known as the start-up region, the wind speed is very low and there is insufficient torque to drive the turbine. When the wind speed is high enough, the system operation will shift to the partial load region, also known as Region 2. In Region 2, the turbine starts to generate power and it is desirable to capture as much wind energy as possible [8-11]. As shown in Fig. 6, the level of electrical power output rises rapidly. As wind speed increases, the power reaches the maximum output of the electrical generator. This is called the rated output power and the wind speed at which it occurs is called the rated output speed. When the wind speed exceeds the rated output speed, the turbine cannot further increase its speed or power generation and shifts to Region 3. In Region 3, the turbine often maintains a constant speed and constant rated power, which is achieved by pitching its blades in order to shed additional wind energy [12-14]. As the wind speed keeps increasing, the forces applied to the turbine structure continue to rise and, at some point, there is a risk of damage to the rotor. As a result, the wind turbine will be shut down in Region 4. This occurs at the cut-out speed.

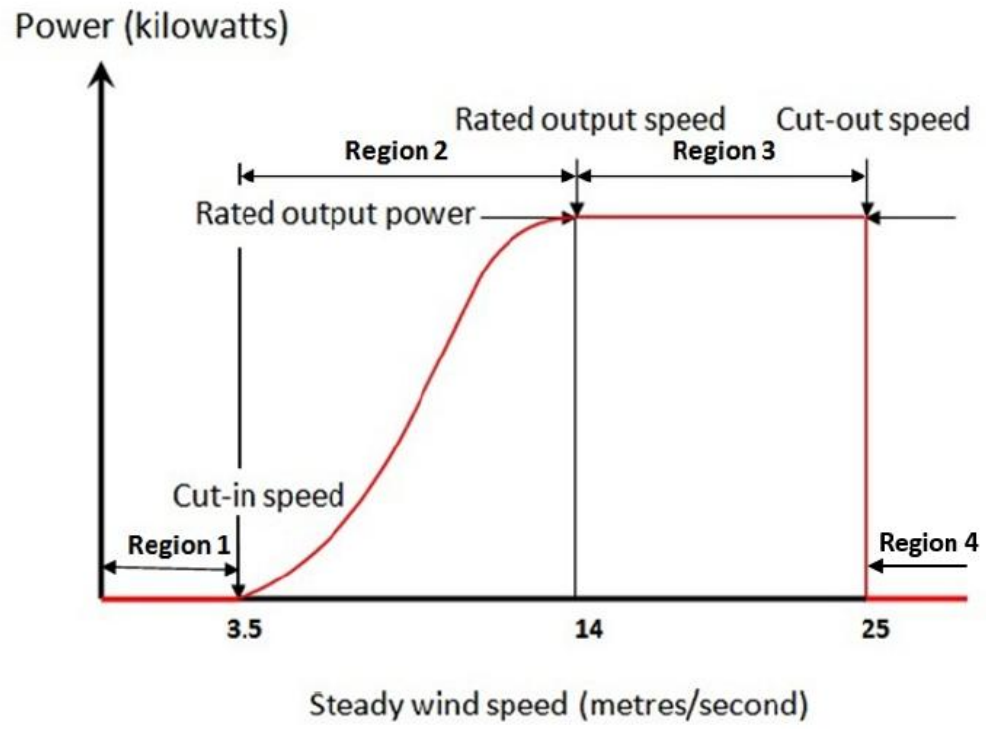

Figure 6: Regions of operation of a wind turbine [7].

Among the four operating regions, Region 2 has drawn much attention because the control implemented into a wind turbine significantly impacts wind energy capture, thus the overall wind turbine efficiency [8-11]. During this region, a variable speed wind turbine can seek maximum wind energy capture by controlling the blade pitch angle and generator torque. Our research mainly focuses on Region 2 operation.

TYPES OF WIND TURBINE CONTROLLERS

A well-designed controller plays a key role in improving wind turbine's efficiency. Controllers for modern wind turbine systems can be classified into two main categories: online and offline controllers. The control algorithms designed for online controllers are

usually simple and the computational expense associated with them is relatively low. Therefore, the online controllers can be easily implemented for real-time control. Typical examples of the control algorithms for online controllers are the traditional torque feedback control method used in Region 2 operation and the PI control used in Region 3 operation. A control block diagram for a wind turbine system using an online controller is shown in Fig. 7. On the other hand, the control algorithms designed for offline controllers are usually more complex, but tend to be more powerful and are able to realize more sophisticated functions. Due to the high computational expense associated with the complex algorithms designed for offline controllers, numerical calculations are performed offline and the resulted control input trajectories are made into look-up tables, which can be used for as feedforward maps for real-time control. A classic example of offline control is the model predictive control method and various algorithms can be embedded into it to realize different functions. A control block diagram for a wind turbine system using an offline controller is shown in Fig. 8.

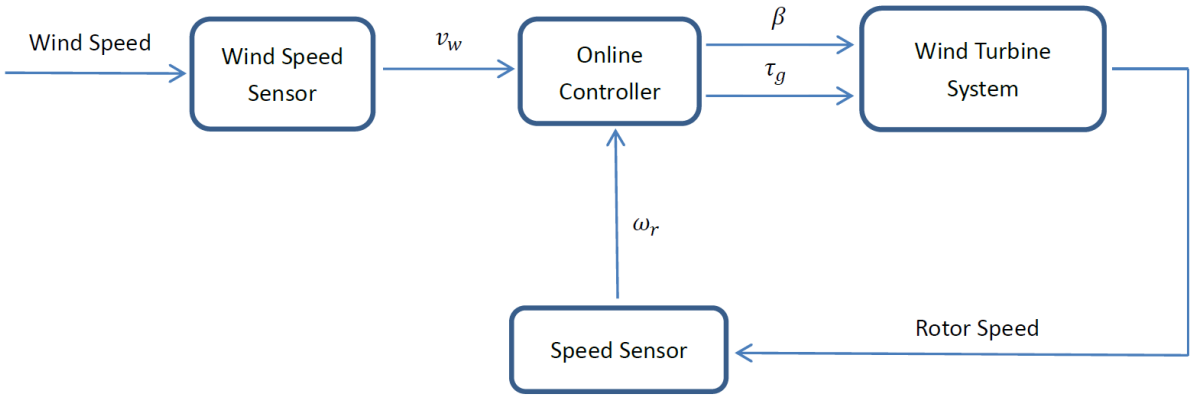

Figure 7: Control block diagram for a wind turbine system using an online controller.

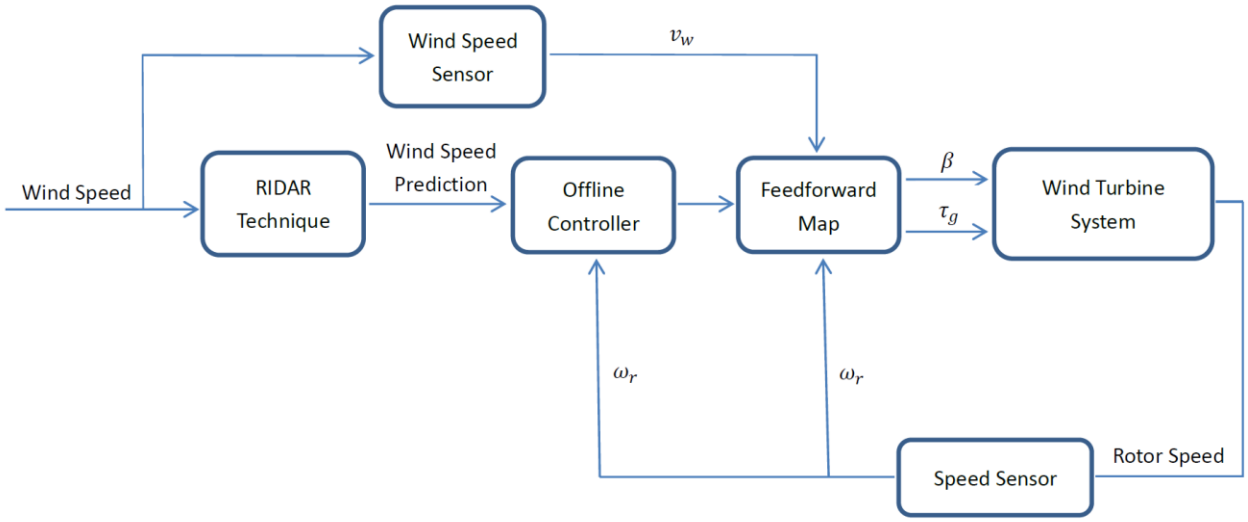

Figure 8: Control block diagram for a wind turbine system using an offline controller.

Chapter 2: *Literature Survey*

Various control algorithms have been developed for wind turbine system to realize different purposes. For Region 2 control, the main control objective is to maximize the overall wind energy capture; For Region 3 control, the main research objective is to regulate turbine speed and maintain the turbine output power as the rated power. In this chapter, a literature survey on the existing control methods for wind turbine system is presented.

REGION 2 CONTROL

The main control objective is for Region 2 operation is to maximize the wind energy capture. In [8-11], a torque feedback control method is mentioned, which is mainly used for Region 2 control. In this torque feedback control method, the turbine generator torque is controlled as a function of rotor speed, which will drive the system to track the maximum aerodynamic power coefficient, thus maximizing the wind energy capture. This method can be easily applied with satisfying performance. Details of this feedback method will be discussed in Chapter 5.

In addition, advanced control methods are also discussed. For Region 2, research is further divided between investigations that incorporate detailed models of the generator electromechanical system and power electronics and those that view the generator torque in terms of a static gain that responds instantly to commanded torque. When studies involve electromechanical models, advanced research congregates around maximum power point tracking (MPPT) [18-23] and sliding mode approaches [24-25]. On the other hand, multi-input-multi-output (MIMO) methods [8-11] tend to be the most prevalent in the research of advanced controls for Region 2, but adaptive [26-30] and novel gain-scheduling [31-32] approaches are also investigated.

The maximum power point tracking algorithms researched so far for the wind turbine system can be classified into three main control methods, namely tip speed ratio (TSR) control, power signal feedback (PSF) control and hill-climb search (HCS) control [18-23]. The TSR control method regulates the rotational speed of the generator in order to maintain the TSR to an optimum value at which the power extracted is maximum; In PSF control, it is required to have the knowledge of the wind turbine's maximum power curve, and track this curve through its control mechanisms; The HCS control algorithm continuously searches for the peak power of the wind turbine. It can overcome some of the common problems normally associated with the other two methods. As mentioned, the MPPT method involves detailed models of the generator electromechanical system and power electronics. The dynamics of these components increases the degree of freedom of the system, also the level of difficulty for the control design.

The sliding mode control method is proposed to ensure the stability of the wind turbine in both Region 2 and Region 3 operations [24-25]. It can also impose the ideal feedback control solution in spite of model uncertainties. The sliding mode control can be further combined with the adaptive control method to update the sliding gain so that better system performance can be achieved [25]. Same as the MPPT method, the sliding mode control method also involves detailed models of the generator electromechanical system and power electronics.

The adaptive control technique can address the inaccuracies in system parameters or the uncertainties in turbine's operating conditions by adapting controller gains to correct them. A small number of papers have been published regarding adaptive control of wind turbines [26-30], but most involve Region 3 control, and very few attempts have been made to test these advanced controls on real turbines. The control law is defined separately for positive and negative regions of the rotor speed because it is undesirable to apply torque

control when the turbine is spinning in reverse. The simulation of this adaptive method shows that the adaptation behavior with the longer adaption period is significantly better than the behavior with the shorter adaption period. Stability analysis is also used for the adaptive control to prove the convergence.

The gain scheduling approach consists in designing linear controllers for several operation points and then applies an interpolation strategy to obtain the global control [31-32]. Consequently, powerful tools for linear systems can be applied to nonlinear plants. The main disadvantage of the gain scheduling method is that linearization needs to be applied about several equilibriums, which requires a relatively stable wind condition. When the wind speed becomes volatile, the gain scheduling method doesn't have a good performance.

Besides maximizing wind energy capture, reducing the harmful effect associated with turbine's operation is another area that draws attention. In [33], a controller is designed to investigate the fatigue loading inflicted on turbine's structure. Research on reducing the noise associated with turbine's operation is also conducted by some researchers.

REGION 3 CONTROL

The control objective for Region 3 operation, which is to regulate turbine speed and maintain generator output power, is easier to realize compared to that of Region 2. Therefore, control design for Region 3 operation is not as sophisticated as Region 2 and some common methods are used. In [8-11], a classical proportional-integral (PI) control technique is introduced for the design of the blade pitch controller for Region 3 operation. This PI control method is used in Region 3 to regulate turbine speed in the presence of varying wind conditions. Further discussions on methods for choosing the gains are found

in [17]. It is also revealed that the standard PI control can be augmented with notch transfer functions to add damping to known resonances.

Adaptive control method can also be applied for Region 3 control. In [29], an adaptive control law is designed to keep the generator torque and rotor speed constant. It is proved that the error caused by a step disturbance can be canceled by the proposed adaptive control law.

SWITCHING CONTROL

A relatively new topic, which starts to draw attention during the recent years, is the switching stability and control of the wind turbine system [34-51]. Depending on the wind speed and the load power demand. The wind turbine's operation could switch between two modes: a multi-input-single-output (MISO) mode and a single-input-single-output (SISO) mode. When switching takes place during turbine's operation, the stability of the switched wind turbine system should be considered at the first place. In [34], the open-loop stability and the closed-loop stability of the switched wind turbine system were both explored based on the famous converse Lyapunov theorems to find the common quadratic Lyapunov function (CQLF) [34-38]. It is found that the open-loop system is asymptotically stable under arbitrary switching and the necessary and sufficient condition for the closed-loop system to be stable can be established within some well-defined regions.

There are not many literatures addressing the control of a switched wind turbine system. The most common strategy is to apply existing control methods to each of the corresponding mode. In [34], it is addressed that the traditional torque feedback control method is applied to maximize the wind energy capture in the MISO mode and the PI control on the blade pitch angle is applied to regulate turbine generator output power in the SISO mode.

Chapter 3: *Research Objectives and Motivations*

Our proposed research focuses on the following three objectives:

1. Maximizing wind energy capture for speed-constrained wind turbines during Region 2 operation.
2. Reducing turbine generator torque variation using time-varying weighting.
3. Maximizing wind energy capture for a switched wind turbine system.

In our research, numerical optimal control method was first applied to maximize the wind energy captured by a speed-constrained wind turbine during Region 2 operation. Then, the approach of time-varying weighting is combined with the numerical optimal control method to reduce the variation in the turbine generator torque trajectory. Finally, the numerical optimal control method is applied to a switched wind turbine system to maximize the wind energy capture. Details about the motivation of each research objective will be introduced in the following sections.

MAXIMIZE WIND ENERGY CAPTURE FOR SPEED-CONSTRAINED WIND TURBINES DURING REGION 2 OPERATION

During Region 2 operation, a wind turbine can seek the maximum wind energy capture by tracking the maximum value of the aerodynamic power coefficient. Control algorithms have been developed for the partial load region to seek the maximum power coefficient [8-11]. Among them, controllers relying on feedback of the global maximum aerodynamic power coefficient are widely used. Despite their good performance and simple implementation, these controllers assume the knowledge of the global maximum power coefficient is always available. Unfortunately this assumption does not apply to all wind turbine systems, especially because requirements for long service lives and inexpensive electronic components impose limits on generator speeds [52-54]. Table 2 is a summary of features of selected variable-speed wind turbines [52] and Tables 3a and 3b

show the turbine operation data from different manufacturers [53]. From Tables 2, 3a and 3b, it can be seen that different turbine models have different ranges of generator speed. Furthermore, in order to avoid resonance effect on wind turbine structure fatigue, several control algorithms have been developed recently to limit the turbine operation speed [55]. These constraints, in addition to the inherent variability of wind speed, can lead to situations where the global maximum of the power coefficient and the ideal turbine speed are not achievable. Such situations pose serious challenges for the aforementioned control algorithms.

Wind Turbine			Generator Description			Power Electronics Modules		
Turbine Name	Date of First Turning	Variable-Speed Range (rpm)	*Class	*Subclass	Stator Pole Count	Rectifier AC→ DC	*Link Type	Inverter DC→AC
AWT-26	August 1998	32 to 60	Induc	WR	4	Rotor Terminal -20→+20 Hz	Resonant	Utility Output 3ϕ, 480v, 60 Hz IGBT
Bergey Excel	1983	0 to 350	Synch	PM	38	Controlled SCR 3ϕ Bridge	300-v. DC Voltage Source	Line commutated 1ϕ, 240 v.
Enercon E-40	1993	15 to 37	Synch	DC	84	Not Available	Not Available	Not Available
EOLE Cap Chat	July 1987	7.9 to 13.5	Direct-Drive Synch	DC	(Large)	Not Available	Not Available	Not Available
Gamma 60	6/03/92	15 to 44	Synch	DC	12	Not Available	DC	3ϕ
Growian	Summer 1983	15 to 21.3	Induc	WR		(na)	Cyclo-Converter	(na)
KENETECH KVS-33	June 1995	Not Available	Induc (Two)	Cage	4	PWM IGBT	DC Voltage	PWM IGBT
Plum Brook MOD-0	March 1986	25 to 37.5	Induc	WR20	4	3ϕ Diode Bridge	DC Voltage	12 pulse Line comm. SCR
DOE Mod-5B	July 1987	12.9 to 17.3	Induc	WR	4	(na)	Cyclo-Converter	(na)
Nordic 400	August 1992	20 to 38	Induc	WR	4	Not Available	DC	Grid Commutated
Northwind 100	1998	Not Available	Synch	WR	4	Not Available	Not Available	Line
Sandia 34-m VAWT	Spring 1987	25 to 38	Synch	WR	4	6-pulse Line comm SCR	DC Current	6 pulse Line comm. SCR
Tvind 54 M	1977	14 to 24	Synch 3 kV	WR	8	3ϕ Diode Bridge	DC, Current	6-pulse Line comm. Thyristor

Table 2: Summary of features of selected variable-speed turbines [52].

Turbine, by manufacturer	Concept[a]	Power and speed control features	Comments
Vestas, Denmark:			
V80, 2.0 MW	Type C1	Pitch Limited variable speed	WRIG (DFIG concept) Generator voltage: 690 V Generator speed range: 905–1915 rpm Rotor speed range: 9–19 rpm
V80, 1.8 MW	Type B1	Pitch Limited variable speed	WRIG Generator voltage: 690 V Generator speed range: 1800–1980 rpm Rotor speed range: 15.3–16.8 rpm
Enercon, Germany:			
E112, 4.5 MW	Type D1	Pitch Full variable speed	Multiple WRIG Generator voltage: 440 V Generator and rotor speed range: 8–13 rpm
E66, 2 MW	Type D1	Pitch Full variable speed	Multiple WRIG Generator voltage: 440 V Generator and rotor speed range: 10–22 rpm
NEG Micon, Denmark:			
NM80, 2.75 MW	Type C1	Pitch Limited variable speed	WRIG (DFIG concept) Generator stator/rotor voltage: 960 V/690 V Generator speed range: 756–1103 rpm Rotor speed range: 12–17.5 rpm
NM72, 2 MW	Type A2	Active stall Fixed speed	SCIG Generator voltage: 960 V Two generator speeds: 1002.4 rpm and 1503.6 rpm Two rotor speeds: 12 rpm and 18 rpm
Gamesa, Spain:			
G83, 2.0 MW	Type C1	Pitch Limited variable speed	WRIG Generator voltage: 690 V Generator speed range: 900–1900 rpm Rotor speed range: 9–19 rpm
G80, 1.8 MW	Type B1	Pitch Limited variable speed	WRIG (OptiSlip® concept) Generator voltage: 690 V Generator speed range: 1818–1944 rpm Rotor speed range: 15.1–16.1 rpm
GE Wind, USA:			
GE 104, 3.2 MW	Type C1	Pitch Limited variable speed	WRIG (DFIG concept) Generator stator/rotor voltage: 3.3 kV/690 V Rotor speed range: 7.5–13.5 rpm Generator speed range: 1000–1800 rpm
GE 77, 1.5 MW	Type C1	Pitch Limited variable speed	WRIG Generator voltage: 690 V Rotor speed range: 10.1–20.4 rpm Generator speed range: 1000–2000 rpm
Bonus, Denmark:			
Bonus 82, 2.3 MW	Type A2	Active stall Fixed speed	SCIG Generator voltage: 690 V Two generator speeds: 1000 rpm and 1500 rpm Two rotor speeds: 11 rpm and 17 rpm
Bonus 76, 2 MW	Type A2	Active stall Fixed speed	SCIG Generator voltage: 690 V Two generator speeds: 1000 rpm and 1500 rpm Two rotor speeds: 11 rpm and 17 rpm

Table 3a: Turbine operation data from different manufacturers all over the world [53].

Turbine, by manufacturer	Concept[a]	Power and speed control features	Comments
Nordex, Germany:			
N80, 2.5 MW	Type C1	Pitch Limited variable speed	WRIG (DFIG concept) Generator voltage: 660 V Generator speed range: 700–1300 rpm Rotor speed range: 10.9–19.1 rpm
S77, 1.5 MW	Type C1	Pitch Limited variable speed	WRIG (DFIG concept) Generator voltage: 690 V Generator speed range: 1000–1800 rpm Rotor speed range: 9.9–17.3 rpm
Made, Spain:			
Made AE-90, 2 MW	Type D1	Pitch Full variable speed	WRSG Generator voltage: 1000 V Generator speed range: 747–1495 rpm Rotor speed range: 7.4–14.8 rpm
Made AE-61, 1.32 MW	Type A0	Stall Fixed speed	SCIG Generator voltage: 690 V Two generator speeds: 1010 rpm and 1519 rpm Two rotor speeds: 12.5 rpm and 18.8 rpm
Repower, Germany:			
MM 82, 2 MW	Type C1	Pitch Limited variable speed	WRIG (DFIG concept) Generator voltage: 690 V Generator speed range: 900–1800 rpm Rotor speed range: 10–20 rpm
MD 77, 1.5 MW	Type C1	Pitch Limited variable speed	WRIG (DFIG concept) Generator voltage: 690 V Generator speed range: 1000–1800 rpm Rotor speed range: 9.6–17.3 rpm
Ecotecnia, Spain:			
Ecotecnia 74, 1.67 MW	Type C1	Pitch Limited variable speed	WRIG (DFIG concept) Generator voltage: 690 V Generator speed range: 1000–1950 rpm Rotor speed range: 10–19 rpm
Ecotecnia 62, 1.25 MW	Type A0	Stall Fixed speed	SCIG Generator voltage: 690 V Two generator speeds: 1012 rpm and 1518 rpm Two rotor speeds: 12.4 rpm and 18.6 rpm

Table 3b: Turbine operation data from different manufacturers all over the world [53].

There are a few algorithms that have been developed to avoid relying upon the global maximum power coefficient, such as adaptive torque control [26-30] and Hill-Climb Search methods [18-23]. These methods greatly enhance wind turbine efficiency in the partial load region, but generally take a long time to converge and are more suitable for

applications where the wind speed input is steady or slowly changing. When the wind speed is more variable, the energy capture capability is not fully realized with these methods. With increased demands on wind power generation, more turbines will be installed at sites with more volatile wind conditions. Accordingly, it will be necessary to develop an optimal controller that maximizes the wind power generation under these conditions.

Optimal control algorithms can be used to control wind turbine future behavior based on a nonlinear turbine model and historic wind speed data [55-56]. The resulting control inputs can be summarized into feedforward maps for real-time control. More importantly, the wind energy captured under this optimal control law will provide a benchmark as the best performance for future control design. Another benefit of employing an optimal control algorithm is that it can be used to size a wind turbine for a specific wind site during the turbine design stage. The integration of optimal control and turbine design leads to an overall efficient wind turbine system.

There are various methodologies that are suitable for time horizon optimization [57-68]. They can be classified into two categories: analytical and numerical methods. When using the analytical method, the general optimal control problem is converted into a two-point boundary value problem (TPBVP) and it is necessary to solve a series of differential equations [58]. Because the mathematical model of the turbine power coefficient is highly complicated, it is difficult if not impossible to solve the optimal control problem analytically. Therefore, numerical methods are used in our research.

There are various numerical methods such as direct shooting (DS), collocation, legendre pseudo spectral, and dynamic programming (DP) [57-83]. These numerical methods generally convert the optimal control problem into a parameter optimization problem [60]. The DS method, which employs the sequential quadratic programming algorithm [69-78], is a widely used numerical method because of its simplicity. However,

when a system has multiple local optimal solutions, additional tuning is required to determine an initial iterate that will be sufficient to find the optimal solution. The DP algorithm can be applied to avoid this problem, as it guarantees the global optimal solution without requiring an analogous starting point [79-83]. However, the computational expense associated with DP algorithm is higher; there is a tradeoff between these two approaches. It is desirable to develop an optimal controller that avoids the need for an initial guess while maintaining computational feasibility.

In our research, we present an optimal control framework to maximize the wind energy capture for a speed-constrained wind turbine to operate in the partial load region. DS and DP algorithms are first explored to find the optimal control input trajectories that maximize the wind energy capture. An Augmented DP algorithm is then proposed based on finding the characteristics of the wind turbine aerodynamic power coefficient. This Augmented DP approach avoids the problem of the initial iterate associated with DS approach, and also reduces the computational expense associated with DP algorithm. Comparisons of the above control algorithms against a widely used torque feedback control (TFC) method [8-11] are presented in a simulation environment. Wind energy capture in the partial load region and the computation expense for each algorithm will be discussed. Details about this research objective will be introduced in Chapter 5.

REDUCING TURBINE GENERATOR TORQUE VARIATION USING TIME-VARYING WEIGHTING

When applying the optimal control technique, there could be cases where the optimal control trajectory needs to change abruptly among several different control inputs. A famous example is the Bang-Bang (on-off) optimal control [84-86], in which case the controller switches abruptly between two states. However, this kind of abrupt switching is not desirable for turbine generator torque control. The reason is that changing the turbine

generator torque abruptly will cause shear stress oscillations and result in the risk of fatigue on the turbine generator shaft [87-88]. Therefore, it is necessary to consider the smoothness of the turbine generator torque trajectory when designing the optimal controller to maximize the efficiency of turbine operation.

The approach of time-varying weightings has been applied to hard disk servo control for generating the optimal actuator seek profile [89]. Comparing to the traditional optimal approaches using constant weightings, it is more effective for minimizing the seek-settling vibration induced by the seek profile and therefore reducing the excitation to the head-stack-assembly (HSA) [89]. The same concept can be applied to our optimal control design to seek further improvement on the smoothness of the turbine generator torque trajectory. Furthermore, the incorporation of time-varying weightings to the optimal control design will provide more design flexibility because different types of functions can be chosen for the time-varying weightings to satisfy different design requirements.

In our research, the performance index of the numerical optimal control method is modified and constant weightings are tuned to investigate the tradeoff between maximizing the wind energy capture and smoothing the turbine generator torque trajectory. Finally, the approach of time-varying weighting is incorporated with the modified performance index of the numerical optimal control method to seek further improvement on the turbine system performance. Comparisons of all of the aforementioned control designs are also presented in a simulation environment. Details about this research objective will be introduced in Chapter 6.

MAXIMIZE WIND ENERGY CAPTURE FOR A SWITCHED WIND TURBINE SYSTEM

The power generated by the wind turbine varies due to variation in the wind speed. Depending on the load power demand and the wind speed, two possible operation modes

of the wind turbine can be defined [34]. When the wind speed is low, the captured wind power is not sufficient to meet the load power. In this case, the generator torque and the blade pitch angle of the turbine need to be controlled at the same time to maximize the captured wind power and some other energy sources, either renewable or nonrenewable, need to be applied to compensate the power deficiency. Since there are two control inputs, the generator torque and the blade pitch angle of the turbine, and one state output, which is the rotor speed of the turbine; this is defined as the multi-input-single-output (MISO) mode. When the wind speed is high and the captured wind power is sufficient to meet the load power, only the blade pitch angle is used to control the turbine to follow the load power demand. In this case, the only control input is the blade pitch angle of the turbine and the output is still the rotor speed of the turbine; this is defined as the single-input-single-output (SISO) mode. A control block diagram based on the aforementioned two operation modes of the turbine is shown in Fig. 9.

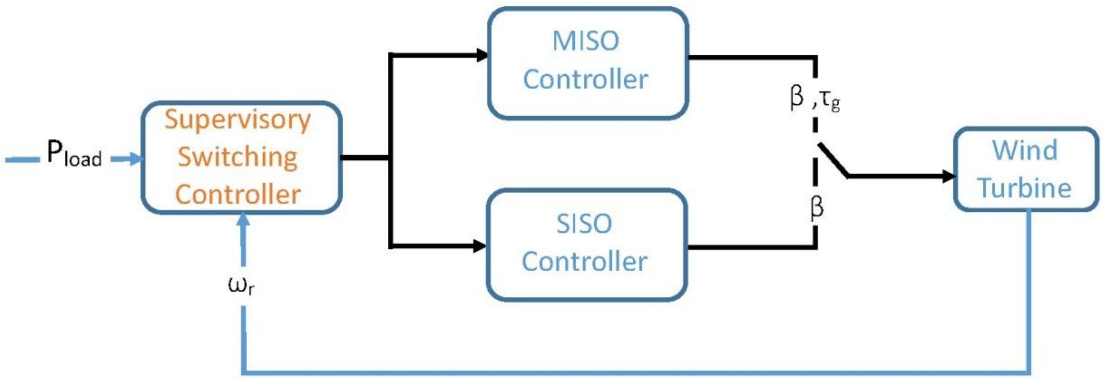

Figure 9: Control block diagram for a switched wind turbine system.

Control algorithms have been developed to improve turbine's efficiency for each corresponding operation mode. For the MISO mode, the control objective is to maximize the wind energy capture and this can be realized by tracking the maximum aerodynamic power coefficient. Algorithms like the traditional feedback control [8-11], the adaptive torque control [26-30] and the maximum-power-point-tracking (MPPT) [18-23] are all able to make the turbine track its maximum power coefficient. For the SISO mode, the control objective is to maintain turbine's generator output power as the load power and this is usually done through a PI control on the blade pitch angle [34]. All of the aforementioned control algorithms provide good performance for the wind turbine system under either specific operation mode. However, when switching between the two modes is involved in turbine's operation, applying the corresponding control algorithms to either specific mode may not provide the overall optimal turbine system performance, especially when the wind speed is volatile or the load power demand is time-varying and multiple switchings happen within a short time period. Therefore, it is necessary to develop an optimal controller that is able to provide the overall optimal turbine system performance when switching is involved in turbine's operation.

In our research, we present an optimal control framework to maximize the overall wind energy capture of a wind turbine system when switching is involved in its operation. The effectiveness of the optimal control design is validated through comparing to the traditional control methods in a simulation environment. The performance of the turbine system is explored under different wind speed inputs and load power demands. Details about this research objective will be introduced in Chapter 7.

Chapter 4: *Turbine Model Recapture*

TURBINE DYNAMICS

A model that describes the wind turbine dynamics and has been used for control design is summarized here [8-11]. Assuming the drivetrain is rigid and its energy loss is negligible, the dynamics of the wind turbine can be represented by

$$\dot{\omega}_r = \frac{1}{J_r}\left(\tau_{aero} - \tau_c\right) \tag{1}$$

where ω_r is the turbine rotor speed, J_r is the combined rotational inertia of the rotor, gearbox, generator and shafts, τ_{aero} is the aerodynamic torque, which drives the turbine, and τ_c is the reactive torque. The aero dynamic torque is defined as

$$\tau_{aero} = \frac{P_{cap}}{\omega_r} \tag{2}$$

where P_{cap} represents the captured wind power. The relation between the captured wind power P_{cap} and the available wind power P_{wind} is defined by the aerodynamic power coefficient C_p. The aerodynamic coefficient measures how effectively the wind energy can be converted into mechanical energy and is defined as

$$C_p = \frac{P_{cap}}{P_{wind}} \tag{3}$$

The available wind power is given by

$$P_{wind} = \frac{1}{2}\rho_{air} A_r v_w^3 \tag{4}$$

where ρ_{air} is the density of air and v_w is the wind speed. A_r is the rotor swept area, defined as

$$A_r = \pi R_r^2 = \frac{1}{4}\pi D_r^2 \tag{5}$$

where R_r is the turbine rotor radius and D_r is the rotor diameter.

The reactive torque in Eqn. (1) is defined as follows

$$\tau_c = \tau_g G_r \tag{6}$$

where τ_g is the turbine generator torque and G_r is the gearbox gear ratio defined as the generator shaft speed over the rotor shaft speed.

By combining Eqns. (1) through (6), the equation which represents the dynamics of the wind turbine can be derived

$$\dot{\omega}_r = \frac{1}{J_r}\left(\frac{\pi}{8} D_r^2 \rho_{air} C_p \frac{v_w^3}{\omega_r} - \tau_g G_r\right) \tag{7}$$

Based on Eqns. (2) through (5), the total wind energy capture over a time interval can be calculated as

$$E_{cap} = \int_{t_0}^{t_f} P_{cap} dt = \int_{t_0}^{t_f} P_{wind} \cdot C_p dt = \frac{\pi}{8}\rho_{air} D_r^2 \cdot \int_{t_0}^{t_f} v_w^3 \cdot C_p dt \tag{8}$$

Since the wind speed is considered a system disturbance and cannot be controlled, maximizing energy capture is equivalent to maximizing the integration of achievable C_p.

AERODYNAMIC POWER COEFFICIENT

The aerodynamic power coefficient C_p is a nonlinear function of the blade pitch angle β and the tip speed ratio λ

$$C_p = f(\lambda, \beta) \tag{9}$$

The tip speed ratio is defined as the linear velocity of the rotor over wind speed and is given by

$$\lambda = \frac{\omega_r D_r}{2v_w} \tag{10}$$

A formula has been developed to approximate the power coefficient [15-16]

$$C_p = c_1\left(\frac{c_2}{\lambda_i} - \mathrm{c}_3\,\beta - \mathrm{c}_4\,\beta^x - \mathrm{c}_5\right)\mathrm{e}^{-\frac{c_6}{\lambda_i}} \tag{11}$$

where

$$\lambda_i = \frac{1}{\lambda + 0.08\beta} - \frac{1}{\beta^3 + 1} \tag{12}$$

and c_1 through c_6 and x are constants. The value of c_1 through c_6 and x can be found in [15]. Table 2 shows the value of c_1 through c_6 and x used for our numerical simulations.

Variable	c_1	c_2	c_3	c_4	c_5	c_6	x
Value	0.5	116	0.4	5	19	0.08	3

Table 4: Values of c_1 through c_6 and x.

The surface plot shown in Fig. 10 illustrates how the power coefficient, C_p, varies with changes in the blade pitch angle, β, and the tip speed ratio, λ. From Fig. 10, it is seen that the plot is a three dimensional surface with complex shape. Due to the dynamics of the turbine, its operation point may slide on this three dimensional surface. However, as revealed by Eqn. (8), in order to maximize the wind energy capture, the aerodynamic power coefficient needs to track the maximum point of this three dimensional surface.

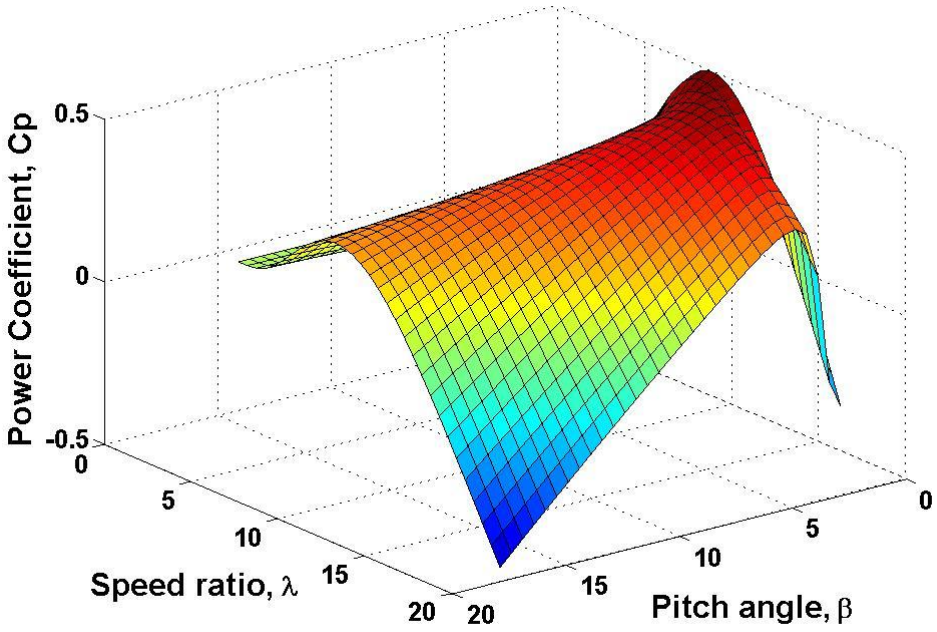

Figure 10: Surface plot of C_p vs. λ and β.

A two dimensional plot of C_p as a function of λ and β is shown in Fig. 11. Each C_p curve corresponds to a different value of β. The thicker black curve consists of multiple segments that represent the maximum possible values of C_p over the ranges of λ and β. Each segment may correspond to a different β depending on the value of λ. The plot shows that a pitch angle of 15° or 25° produces the maximum achievable power coefficient at low values of λ, i.e., $\lambda < \lambda_a$ in Fig. 11. For high values of λ, i.e., $\lambda > \lambda_b$ in Fig. 11, achievable maxima of C_p are generated by pitch angles of 1° or 2°. For the range of λ between λ_a and λ_b in Fig. 11, all of the achievable maxima of C_p are on the 0° pitch angle curve, including the global maximum of C_p, $(C_p)_{max}$, and its corresponding λ value is labeled as λ_*. Due to constraints governed by the rotor speed and wind speed, the global maximum of C_p is not always achievable. In this case, the

achievable maximum of C_p can only be obtained by tuning β appropriately. These constraints will be mathematically defined later.

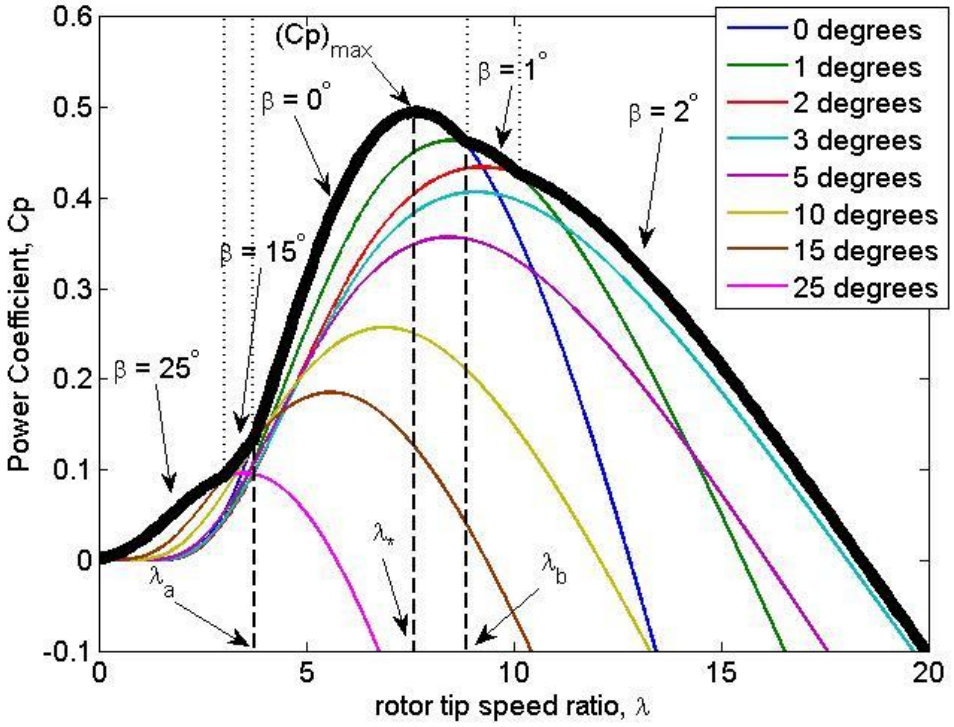

Figure 11: Plot of the aerodynamic power coefficient versus the rotor tip speed ratio with different blade pitch angles.

It has been shown that maximizing the wind energy capture is equivalent to maximizing the integral term in Eqn. (8). For the case of steady-state operation, C_p should be kept as its global maximum value to maximize the wind energy capture. However, due to the variation in wind speed or the constraint on rotor speed, the transient of the turbine may cause λ to fall into any region of the horizontal axis in Fig. 11. In this case, in order

to maximize the integral term in Eqn. (8), β needs to be tuned to make the turbine always pursue the achievable maximum of C_p during its transient.

Chapter 5: *Maximizing Wind Energy Capture for Speed-Constrained Wind Turbines during Partial Load Operation*[1-2]

In this chapter, we present an optimal control framework to maximize the wind energy capture for a speed-constrained wind turbine to operate in the partial load region. Direct shooting (DS) method [57-63] and dynamic programming (DP) algorithm [79-83] are first explored to find the optimal control input trajectories that maximize the wind energy capture. An Augmented DP algorithm is then proposed based on finding the characteristics of the wind turbine aerodynamic power coefficient. This Augmented DP approach avoids the problem of the initial iterate associated with DS approach, and also reduces the computational expense associated with DP algorithm. Comparisons of the above control algorithms against a widely used torque feedback control (TFC) method [8-11] are presented in a simulation environment. Wind energy capture in the partial load region and the computation expense for each algorithm will be discussed.

CONTROL DESIGN FOR REGION 2 OPERATION

Traditional Torque Feedback Control (TFC)

The traditional torque feedback control (TFC) is widely used in industry [8-11]. This control method relies on the feedback of the global maximum power coefficient and assumes the knowledge of the global maximum power coefficient is always attainable. It is considered as a benchmark in this research and its performance will be compared with

---

[1] ***Z. Yan***, ***J.F. Hall***, and ***D. Chen***, 2012," A Dynamic Optimization Approach for Maximum Aerodynamic Coefficient of Wind Turbine Systems," Proceedings of 2012 ASME Dynamic Systems and Control Conference, Ft. Lauderdale, FL, October 17-19.

[2] ***Z. Yan***, ***J.F. Hall***, and ***D. Chen***, 2013," MIMO control of Wind Turbine Using Direct Shooting Method," Proceedings of 2013 American Control Conference, Washington DC, June 17-19.

The corresponding authors John Hall and Dongmei Chen provided precious research advice for the above publications.

that of the proposed optimal control law.

For traditional TFC method, the turbine generator torque is controlled according to a feedback control law [8-11], described as follows

$$\tau_c = \tau_g G_r = K_\tau \omega_r^2 \tag{13}$$

where K_τ has the following form

$$K_\tau = \frac{1}{2}\rho_{air}\pi R_r^{\,5}\frac{(C_p)_{max}}{\lambda_*^3} = \frac{1}{2}\rho_{air}\pi R_r^{\,5}\frac{C_p(\lambda_*,\beta_*)}{\lambda_*^3} \tag{14}$$

where $(C_p)_{max}$ is the global maximum value of C_p and λ_* and β_* are the corresponding values of λ and β to $(C_p)_{max}$ in Fig. 8.

By substituting Eqn. (14) into Eqn. (7), the following equation is derived

$$\dot{\omega}_r = \frac{1}{2J_r}\rho_{air}\pi R_r^5\omega_r^2\left[\frac{C_p}{\lambda^3} - \frac{(C_p)_{\max}}{\lambda_*^3}\right] \tag{15}$$

It is clear that $\dot{\omega} < 0$ when $C_p < \frac{(C_p)_{\max}}{\lambda_*^3}\lambda^3$ and $\dot{\omega} > 0$ when $C_p > \frac{(C_p)_{\max}}{\lambda_*^3}\lambda^3$. Thus this control law causes the turbine to accelerate toward the desired set point when the rotor speed is slow and decelerate when the rotor speed is too fast. As a result, this generator torque control law will balance the aerodynamic and load torques to regulate the speed of the turbine to the optimal tip speed ratio in steady-state conditions.

On the other hand, the blade pitch angle is controlled to track β_* as follows

$$\frac{d\beta}{dt} = K_\beta(\beta_* - \beta) \tag{16}$$

where K_β is a positive gain which can be tuned to control the speed of tracking.

Optimal Control Design

General Form

A general form of an optimal control problem is defined as follows

$$\min \quad J = \phi\left(t_f, \vec{\mathrm{x}}_f\right) \tag{17}$$

where *J* is the performance index to be minimized, subject to the differential constraints, which are usually the state equations of the system

$$\frac{d\vec{x}(t)}{dt} = \vec{f}\left[t, \vec{x}(t), \vec{u}(t)\right] \tag{18}$$

and the following initial and finial conditions, and constraints

$$\begin{aligned} t_0 &= t_{0_s} \\ \vec{x}_0 &= \vec{x}_{0_s} \\ \vec{\psi}\left(t_f, \vec{x}_f\right) &= 0 \\ \vec{\theta}\left(t_f, \vec{x}_f\right) &\le 0 \end{aligned} \tag{19}$$

where *t* stands for time, $\vec{x}$ stands for the state vector and $\vec{u}$ stands for the control vector. t_{0_s} and $\vec{x}_{0_s}$ stand for the initial value of *t* and $\vec{x}$, which are specified according to the initial state of the wind turbine. $\vec{\psi}$ is a $p \times 1$ vector and $\vec{\theta}$ is a $q \times 1$ vector, where *p* and *q* are the numbers of final equality and inequality constraints. The control input and

state inequality constraints also need to be satisfied

$$\begin{aligned}\overrightarrow{CC}\left(t,\vec{x},\vec{u}\right)\le 0\\ \overrightarrow{SC}\left(t,\vec{x},\vec{u}\right)\le 0\end{aligned} \tag{20}$$

where $\overrightarrow{CC}$ denotes the control inequality constraints and is an $m\times 1$ vector; $\overrightarrow{SC}$ denotes the state inequality constraints and is an $n\times 1$ vector. *m* and *n* are the numbers of control and state inequality constraints.

Suboptimal Control Problem

All of the optimal control problems can be converted into parameter optimization problems [60]. This is accomplished by replacing histories of the control input and state with parameters, and reconstructing the histories by interpolation between the parameters. Then various algorithms such as the sequential quadratic programming algorithm [69-78] or the dynamic programming algorithm [79-83] can be used to solve this parameter optimization problem. More details about conversion of optimal control problems into parameter optimization problems can be found in [60].

During the conversion, the first step is to normalize the final time as follows

$$T=\frac{t}{t_f} \tag{21}$$

where *t* stands for time, t_f stands for the final value of *t* .

Thus, the *N* fixed times

$$0 = T_1 < T_2 < \cdots < T_k < \cdots < T_{N-1} < T_N = 1 \tag{22}$$

are called nodes, which are usually equally spaced.

If we change variable from *t* to *T*, the state equation becomes

$$\frac{d\vec{x}(t)}{dT} = t_f \cdot \vec{f}\left(t_f, T, \vec{x}(T), \vec{u}(T)\right) = \vec{g}\left(T, \vec{x}, \vec{u}, t_f\right) \tag{23}$$

Then, functions of time $\vec{u}(T)$ and $\vec{x}(T)$ are replaced by their values at the nodes ($\vec{u}_k$ and $\vec{x}_k$) and the interpolations are used for the control points between nodes. We chose linear interpolation our algorithms due to its simplicity and low computational cost. When using a linear interpolation, the control input between nodes has the following form

$$\vec{u}(T) = \vec{u}_k + \frac{\vec{u}_{k+1} - \vec{u}_k}{T_{k+1} - T_k}(T - T_k), \quad T_k \le T \le T_{k+1} \tag{24}$$

where $\vec{u}_k$ and $\vec{u}_{k+1}$ are the values of the control input vectors at the k^{th} node and $(k+1)^{th}$ node. The visualization of this linear interpolation is shown in Fig. 12.

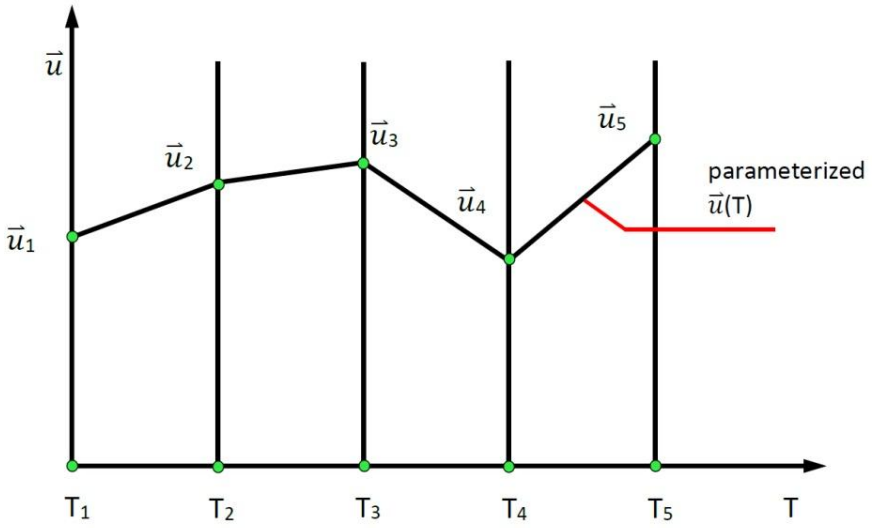

Figure 12: Visualization of linear interpolation between nodes.

Combining Eqns. (23) and (24), it can be seen that the final state is a function of the final time and the values of the control inputs at nodes

$$\vec{x}_f = \vec{x}_f\left(t_f, \vec{u}_1, \vec{u}_2, ..., \vec{u}_N\right) \tag{25}$$

The performance index in Eqn. (17) and all of the constraints in Eqns. (19) and (20) then become

$$
\begin{aligned}
J = \phi\left[\vec{x}_f\left(t_f, \vec{u}_1, \vec{u}_2, ..., \vec{u}_N\right), t_f\right] &:= F\left(t_f, \vec{u}_1, \vec{u}_2, ..., \vec{u}_N\right) \\
\vec{\psi}\left[\vec{x}_f\left(t_f, \vec{u}_1, \vec{u}_2, ..., \vec{u}_N\right), t_f\right] = 0 &:= C_i\left(t_f, \vec{u}_1, \vec{u}_2, ..., \vec{u}_N\right) = 0, \\
& \quad i = 1, ..., p \\
\vec{\theta}\left[\vec{x}_f\left(t_f, \vec{u}_1, \vec{u}_2, ..., \vec{u}_N\right), t_f\right] \le 0 &:= C_j\left(t_f, \vec{u}_1, \vec{u}_2, ..., \vec{u}_N\right) = 0, \\
& \quad j = 1, ..., q \\
\overrightarrow{CC}\left(\vec{u}_1, \vec{u}_2, ..., \vec{u}_N\right) \le 0 &:= C_k\left(\vec{u}_1, \vec{u}_2, ..., \vec{u}_N\right) \le 0, \\
& \quad k = 1, ..., m \\
\overrightarrow{SC}\left(\vec{u}_1, \vec{u}_2, ..., \vec{u}_N\right) \le 0 &:= C_l\left(\vec{u}_1, \vec{u}_2, ..., \vec{u}_N\right) \le 0, \\
& \quad l = 1, ..., n
\end{aligned}
\tag{26}
$$

If $\vec{X}$ denotes the vector of unknown parameters as

$$
\vec{X} = \left[t_f \;\; \vec{u}_1^T \;\; \vec{u}_2^T \;\; \cdots \;\; \vec{u}_k^T \;\; \cdots \;\; \vec{u}_N^T\right]^T \tag{27}
$$

The optimal control problem becomes

$$
\min \;\; J = F\left(\vec{X}\right) \tag{28}
$$

subject to

$$
\begin{aligned}
& C_i\left(\vec{X}\right) = 0, \;\; i = 1, ..., m_e \\
& C_j\left(\vec{X}\right) \le 0, \;\; j = m_e + 1, ..., m_{total}
\end{aligned}
\tag{29}
$$

where C_i and C_j stand for the equality and inequality constraints $\vec{X}$ needs to be satisfied, m_e is the number of equality constraints, m_{total} is the total number of equality constraints plus the number of inequality constraints. Equations (28) and (29) are the

standard forms of a parameter optimization problem. The final task is to find the optimal $\vec{X}$ that minimizes or maximizes the performance index according to control design requirements.

As shown in Chapter 4, to maximize the wind energy capture, the integration in Eqn. (8) needs to be maximized. Therefore, the performance index of our wind turbine optimal control problem has the following form

$$\max \quad J = \int_{t_0}^{t_f} v_w^3(t) \cdot C_p\left[\vec{u}(t)\right] dt \tag{30}$$

Here C_p is written as a function of $\vec{u}(t)$ instead of λ and β because λ is a function of the system state ω_r, which is actually a function of the control inputs.

Based on the nodes defined in Eqn. (22), the performance index for our numerical optimization is defined as follows

$$\max \quad J = \sum_{k=1}^{N-1} \int_{T_k}^{T_{k+1}} v_w^3(T) \cdot C_p\left(\vec{X}, T\right) dT \tag{31}$$

and the unknown parameters $\vec{X}$ has the form

$$\vec{X} = \left[\beta_1 \ \beta_2 \ \cdots \ \beta_k \ \cdots \ \beta_N \ (\tau_g)_1 \ (\tau_g)_2 \ \cdots \ (\tau_g)_k \ \cdots \ (\tau_g)_N\right]^T \tag{32}$$

where β_k and $(\tau_g)_k$ stands for the value of the control inputs β and τ_g at the k^{th} node. The final time is not included in Eqn. (32) because wind turbine's operation time is usually specified.

For certain wind turbines, the generator speed is limited within a certain range [52-55]. This imposes the following constraints on the turbine system

$$\left(\omega_g\right)_{min} \le \omega_g \le \left(\omega_g\right)_{max} \tag{33}$$

Since the turbine generator speed and rotor speed are related by

$$\omega_r = \frac{\omega_g}{G_r} \tag{34}$$

The constraint on turbine generator speed in Eqn. (33) is equivalent to the following constraint on turbine rotor speed

$$\left(\omega_r\right)_{min} \le \omega_r \le \left(\omega_r\right)_{max} \tag{35}$$

The two control inputs, β and τ_g, should also be in proper ranges

$$\begin{aligned} \beta_{min} \le \beta \le \beta_{max} \\ (\tau_g)_{min} \le \tau_g \le (\tau_g)_{max} \end{aligned} \tag{36}$$

The above constraints affect the achievability of the global maximum power coefficient. Due to the constraint on rotor speed, the rotor tip speed ratio, λ, could be smaller than λ_a and larger than λ_b in Fig. 11. Therefore, the global maximum of C_p is not achievable. It should be noted that when the global maximum of C_p is not achievable, both the blade pitch angle and the generator torque need to be tuned to pursue the achievable maxima of C_p. Existing control methodologies that rely on pursuing the global

maximum of C_p will not capture the maximum wind energy. Therefore, it is necessary to explore control algorithms based on searching the achievable maxima of C_p.

After the optimal control problem has been converted into a parameter optimization problem, numerical optimization algorithms can then be applied to solve for the unknown parameters $\vec{X}$ which maximizes that performance index defined in Eqn. (31). Once the optimal parameters are determined, the optimal control input trajectories can be generated using Eqn. (24) and the optimal state output trajectory can be generated by integrating Eqn. (7). Two representative numerical optimization techniques, the sequential quadratic programming algorithm and the dynamic programming algorithm were used to solve the parameter optimization problem in our research.

Numerical Optimization Algorithms

Traditional Algorithms

After the optimal control problem has been converted into a standard parameter optimization problem, optimization algorithms need to be applied to solve for the optimal parameters. The parameter optimization problem actually belongs to the scope of constrained nonlinear programming (NLP) problem [73-78] and various algorithms can be applied to solve it.

There are series of algorithms based on searching the local minima or maxima that are suitable for solving the NLP problems. The most widely used example is the sequential quadratic programming (SQP) algorithm [69-78]. However, this kind of algorithms requires a well-conditioned initial guess to obtain the global optimal solution, especially when the performance index has a complex shape with multiple local minima or maxima. Due to the complexity of the mathematical model of the power coefficient, additional tuning effort on the initial iterate is necessary for our wind turbine optimal control problem.

Searching for a suitable starting point increases the computational expense, and potentially affects the efficiency of this kind of algorithms.

The dynamic programming (DP) algorithm [79-83] can also be used to solve the nonlinear programming problems. Unlike the aforementioned algorithms for searching the local minima or maxima, the DP algorithm always finds the global minimum or maximum without the need for initial guessing. However, in order to use the DP algorithm to find the optimal control input trajectories, the two control inputs, β and τ_g need to be discretized at each node. When there is more than one control input to be discretized, nested loops will be involved in the DP algorithm and make the algorithm computationally expensive. High computational expense is the main disadvantage of the DP algorithm.

The SQP algorithm is available in various software packages, for example, the MATLAB optimization toolbox. On the other hand, there are few software packages available for the implementation of the DP algorithm. In order to use the DP algorithm, one needs to build his own code according to different design requirements. In the next section, the details about the implementation of the DP algorithm to solve our parameter optimization problem are introduced.

DP Algorithm Design

We need to develop our code to apply the DP algorithm to solve the parameter optimization problem. In order to use the DP algorithm, the blade pitch angle and the generator torque are discretized at each node. The vectors which includes the discrete values of β and τ_g are defined as follows

$$\vec{\tau}_g = \left[\left(\tau_g\right)_1 \ \left(\tau_g\right)_2 \ \cdots \ \left(\tau_g\right)_m \right]^T \quad \vec{\beta} = \left[\beta_1 \ \beta_2 \ \cdots \ \beta_n\right]^T \tag{37}$$

where

$$\begin{gathered}\left(\tau_g\right)_{min}=\left(\tau_g\right)_1<\left(\tau_g\right)_2<\cdots<\left(\tau_g\right)_m=\left(\tau_g\right)_{max}\\ \beta_{min}=\beta_1<\beta_2<\cdots<\beta_n=\beta_{max}\end{gathered} \tag{38}$$

and

$$\begin{gathered}\left(\tau_g\right)_{j+1}-\left(\tau_g\right)_j=\Delta\tau_g,\quad 1\le j\le m-1\\ \beta_{p+1}-\beta_p=\Delta\beta,\quad 1\le p\le n-1\end{gathered} \tag{39}$$

where $\Delta\tau_g$ and $\Delta\beta$ are the fixed discretization steps. For smaller choices of $\Delta\tau_g$ and $\Delta\beta$, the simulation will be more accurate. Because we are applying discretization within proper ranges of the control inputs, and linear interpolations are used for control inputs between nodes, the control inequality constraints in Eqn. (36) will always be satisfied. Equation (35) is used to eliminate the improper solutions which violate the turbine rotor speed constraint.

If we define the value function as

$$\begin{gathered}V_{k,h,q}=\max_{\substack{1\le j\le m\\ 1\le p\le n}}\int_{T_k}^{T_{k+1}}v_w^3(T)\cdot C_p\left\{t_f,\begin{bmatrix}\left(\tau_g\right)_j\\ \beta_p\end{bmatrix},\begin{bmatrix}\left(\tau_g\right)_h\\ \beta_q\end{bmatrix},T\right\}dT+V_{k-1,j,p}\\ 2\le k\le N\\ 1\le j,h\le m\\ 1\le p,q\le n\end{gathered} \tag{40}$$

where the subscript *k* stands for the k^{th} node. When the control inputs are discretized, the combinations of β and τ_g at each node can be visualized as a plane. The subscripts *j*, *h*, *p*, and *q* represent the coordinates of the points on the planes, as shown in Fig. 13. Equation (40) is defined for maximizing the cost of going from the start point to the point (*h*, *q*) on

the plane associated with the k^{th} node. The term $V_{k-1,j,p}$ accounts for the cost of the last step. In this way, the cost of each step will be accumulated and stored.

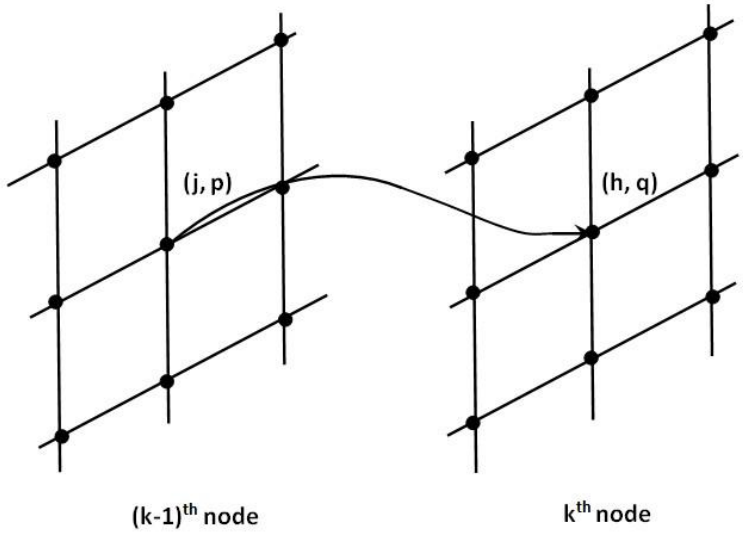

Figure 13: Visualization of the DP algorithm going from the $(k-1)^{th}$ node to the k^{th} node.

Finally, we want to maximize the total cost, which is

$$V_{\text{total}} = \max_{\substack{1\le h\le m \\ 1\le q\le n}} V_{N,h,q} \tag{41}$$

The final conditions are determined by finding the indices h and q at the N^{th}node. Then all of the optimal control trajectories are generated using a back calculation. After the optimal control trajectories are obtained by solving the parameter optimization problem defined by Eqns. (28) and (29), the optimal state trajectories are obtained by integrating the state equations of the system.

The DP algorithm is able to find the global optimal solution without the effort of searching for a good initial guess. However, high computational expense is the main disadvantage of it. An augmented dynamic programming algorithm based on the characteristics of C_p curve is developed by us, which is still able to find the global optimal solution, but with reduced computational expense. The details about the development of the augmented dynamic programming algorithm are introduced in the next section.

Augmented Dynamic Programming (ADP) Algorithm Development

The DP technique will provide a global optimization over a time horizon. However, the wind turbine application has two control inputs to discretize. Nested loops are involved in the DP algorithm, and so the algorithm is computationally expensive. In order to reduce the cost, an augmented DP algorithm is developed based on the location of the rotor tip speed ratio on the horizontal axis. The new approach could significantly reduce the computational time and still generate the same optimization result compared to the traditional DP algorithm.

Recall that in Fig. 11, the tip speed ratio corresponding to the global maximum of C_p is defined by λ_* and the thicker black line is a combination of all of the largest achievable maxima of C_p. It can be seen that the thicker black curve is monotonically increasing with λ when $\lambda \leq \lambda_*$ and monotonically decreasing with λ when $\lambda \geq \lambda_*$. This means that when the available range of λ does not include λ_*, the global maximum of C_p is not reachable and ω_r needs to lie on its upper or low boundary for the maximum C_p value. In mathematical form, we define

$$\lambda_{min} = \frac{(\omega_r)_{min} D_r}{2(v_w)_{max}} \qquad \lambda_{max} = \frac{(\omega_r)_{max} D_r}{2(v_w)_{min}} \tag{42}$$

where $(v_w)_{min}$ and $(v_w)_{max}$ are the minimum and maximum wind speed. Three scenarios will be discussed based on the range and location of the tip speed ratio on the horizontal axis.

(a) If $\lambda_{max} < \lambda_*$, the maximum C_p is achieved when $\lambda = \lambda_{max}$, i.e. $\omega_r = (\omega_r)_{max}$. This is illustrated in Fig. 14. The problem can be divided into two parts. In the first part, β and τ_g need to be controlled simultaneously to make the system reach $(\omega_r)_{max}$ within a minimum amount of time, which can be defined as a minimum final time problem

$$\min \quad J = t_f \tag{43}$$

subject to the following final conditions

$$\begin{aligned} \left(\omega_r\right)_f &= \left(\omega_r\right)_{max} \\ \left(\dot{\omega}_r\right)_f &= 0 \end{aligned} \tag{44}$$

After the rotor speed reaches its maxima, the system enters into the second part where $\omega_r = (\omega_r)_{max}$ will be at steady state. At this point, only β needs to be tuned to achieve optimal system performance. Since ω_r will be at steady state, λ will be a function of only $v_w(t)$. The optimal β trajectory can then be found by using the DP algorithm. Once the optimal pitch angle trajectory, $\beta_{opt}(t)$, is determined, the generator torque trajectory is derived from Eqn. (7) by setting the rotor angular acceleration to zero

$$\dot{\omega}_r = 0 \;\Rightarrow\; \tau_g(t) = \frac{\pi D_r^2 \rho_{\text{air}} C_p\left[\lambda_{bv}(t), \beta_{opt}(t)\right] v_w^3(t)}{8 G_r \left(\omega_r\right)_{max}} \tag{45}$$

where

$$\lambda_{bv}(t) = \frac{\left(\omega_r\right)_{max} D_r}{2 v_w(t)} \tag{46}$$

Since only β needs to be tuned using the DP algorithm during the second part, no nested loops will be involved as in the traditional DP algorithm. Therefore, the running time is much shorter compared to the case where both the control inputs, β and τ_g, need to be tuned.

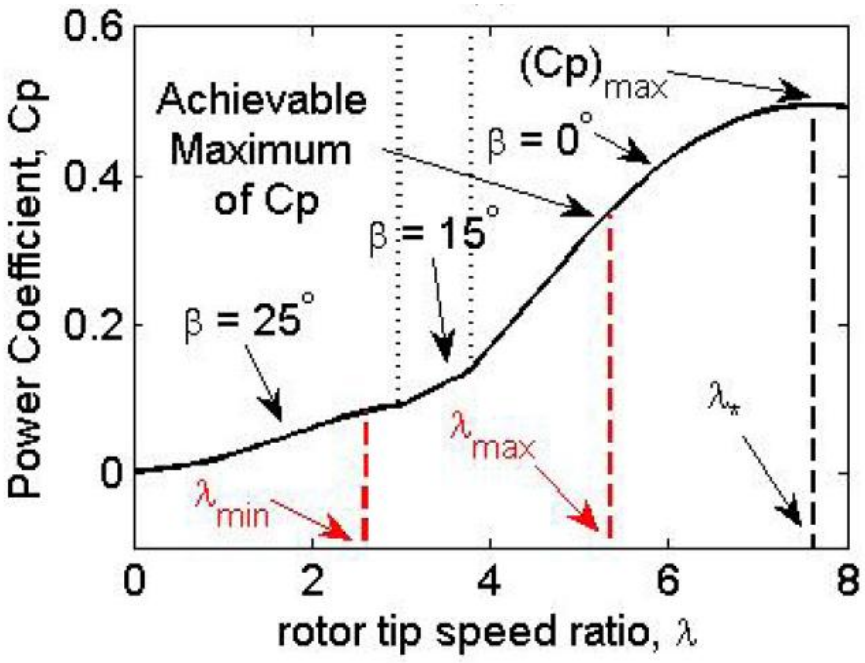

Figure 14: Illustration of ADP development case (a).

(b) If $\lambda_{min} > \lambda_*$, the maximum C_p is achieved when $\lambda = \lambda_{min}$, i.e. $\omega_r = (\omega_r)_{min}$. This is illustrated in Fig. 15. The structure of the algorithm is the same as that of case (a), except that $(\omega_r)_{max}$ in Eqns. (44), (45) and (46) needs to be replaced by $(\omega_r)_{min}$. Applying the same technique used in case (a), the optimal β trajectory to reach the maximum C_p can be obtained.

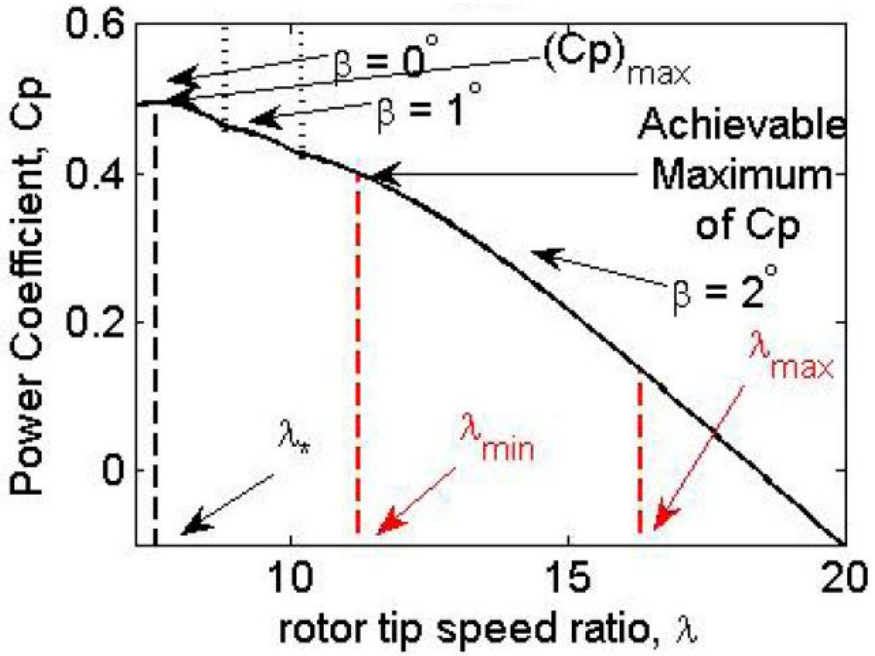

Figure 15: Illustration of ADP development case (b).

(c) If $\lambda_{min} \leq \lambda_* \leq \lambda_{max}$, the global maximum of C_p is reachable. In Fig. 11, it is seen that when $\lambda_a < \lambda < \lambda_b$, all of the achievable maxima of C_p lie on the curve where β is 0°. When $\lambda_a \leq \lambda_{min} \leq \lambda \leq \lambda_{max} \leq \lambda_b$, as shown in Fig. 16, β needs to be kept at 0° and the only control input is the generator torque. Using the DP algorithm will generate the optimal τ_g profile to reach the maximum C_p. Again, only having one

control input, τ_g, significantly reduces the computational expense, which will also reduce the running time of the DP algorithm. If $\lambda_{min} < \lambda_a$ or $\lambda_{max} > \lambda_b$, as shown in Fig. 17, controlling both pitch angle and generator torque is still needed when applying the DP technique.

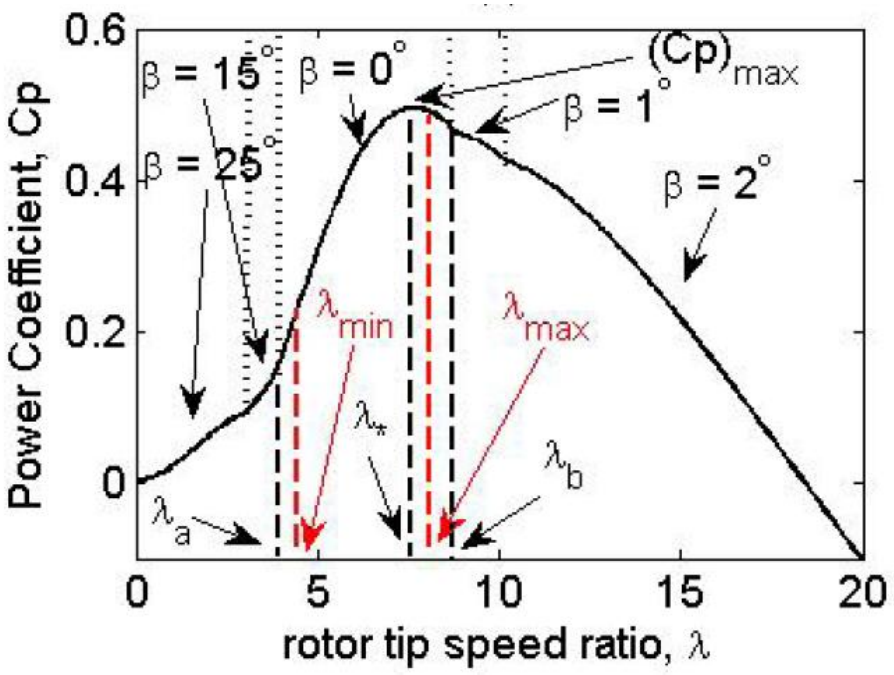

Figure 16: Illustration of ADP development case (c).

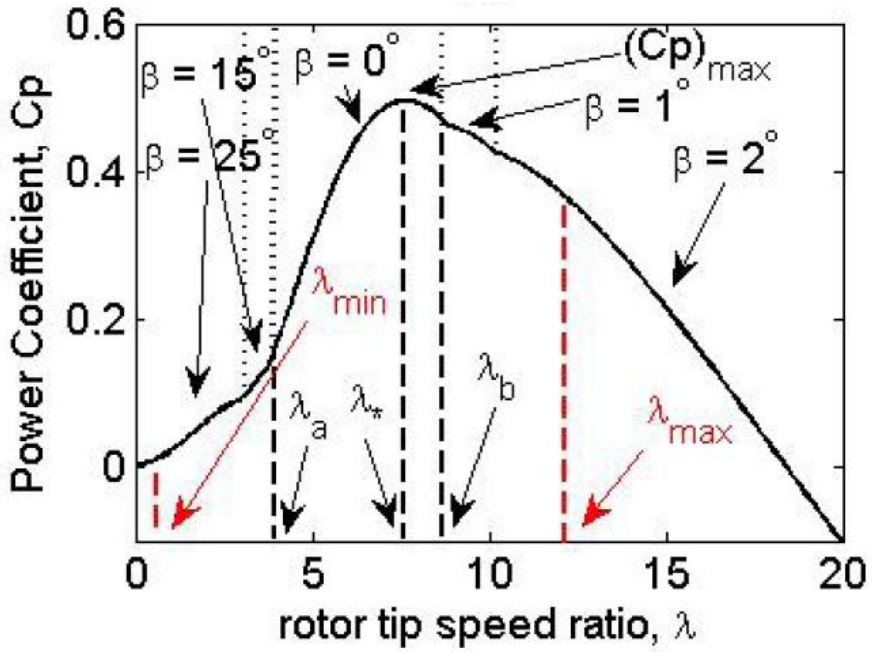

Figure 17: Illustration of ADP development case (c) (continued).

This augmented DP algorithm switches between one input and two inputs controls depending on the tip speed ratio value. It greatly reduces the computational expense and makes the new algorithm potentially applicable for real time control.

Numerical Integrator

After the optimal control input trajectories are determined, the optimal state output trajectories can be generated through integrating the state equations of the system. A numerical integrator is needed to integrate the state equations of the system to generate the optimal state output trajectories. The Runge Kutta (RK) explicit integrators are used in our numerical simulation [90-92]. Explicit means that all information necessary to compute the right hand side of a differential equation is known. Only fixed step integrators are considered.

Consider the system differential equation as

$$\dot{x} = f\left(t, x, u\right) \tag{47}$$

Then the RK integrator has the following form

$$\begin{aligned} x_{i+1} &= x_i + h\sum_{j=1}^{p} c_j f_j \\ f_1 &= f\left(t_i, x_i\right) \\ f_j &= f\left(t_i + h\alpha_j, x_i + h\sum_{\lambda=1}^{j-1} \beta_{j\lambda} f_\lambda\right), \quad j \geq 2 \end{aligned} \tag{48}$$

where p is the number of function evaluations to be used, c, α and β are constants to determined. To determine the values of the constants, c, α and β, we need to first specify p and assume h is small, then expand the RK assumption in a taylor-series (TS) and compare the RK expansion with the exact TS expansion.

The exact TS expansion is given as follows

$$x_{i+1} = x\left(t_i + h\right) = x\left(t_i\right) + \dot{x}\left(t_i\right)h + \frac{1}{2!}\ddot{x}\left(t_i\right)h^2 + \cdots \tag{49}$$

where

$$\dot{x}\left(t_i\right) = f\left(t_i, x_i\right) \tag{50}$$

Since

$$\ddot{x} = f_t + f_x \dot{x} \tag{51}$$

where f_t and f_x are notations of the partial derivative of *f* with respect to *t* and *x*.

$$f_t := \frac{\partial f}{\partial t} \qquad f_x := \frac{\partial f}{\partial x} \tag{52}$$

therefore we have

$$\ddot{x}(t_i) = (f_t)_i + (f_x)_i (f)_i \tag{53}$$

For an n^{th} order integrator, the RK TS matches the exact TS through terms of order h^n. Table 5 shows the α and β values of the 4^{th} order RK integrator, which is used in our numerical simulations [90-92].

α_i	β_{ij}
$\alpha_1 = 0$	$\beta_{21} = 1/2$
$\alpha_2 = 1/2$	$\beta_{32} = 1/2$
$\alpha_3 = 1/2$	$\beta_{43} = 1$
$\alpha_4 = 1$	$\beta_{ij} = 0$ otherwise

Table 5: α and β values of the 4^{th} order RK integrator [90-92].

SIMULATION RESULTS AND ANALYSIS

Simulations were conducted to evaluate the performance of the above control algorithms with respect to wind energy capture. Turbine system parameters used for the simulations are provided in Table 6. For comparison purpose, the performance of the proposed control methods are compared to the traditional torque feedback control (TFC) method [8-11], which is widely used in industry. Wind speed in the forms of a step input and a continuous input are used to test the system performance.

Parameters	Value
Turbine rated power, P_{rated}	100 kW
Rotor moment of inertia, J_r	2.6×10^4 kg · m^2
Rotor diameter, D_r	18.50 m
Gear ratio, G_r	21.5858
Maximum generator angular speed, $(\omega_g)_{max}$	1800 RPM×130%
Minimum generator angular speed, $(\omega_g)_{min}$	1800 RPM×70%
Maximum blade pitch angle, β_{max}	25 degree
Minimum blade pitch angle, β_{min}	0 degree
Maximum Generator input torque, $(\tau_g)_{max}$	3000 Nm
Minimum Generator input torque, $(\tau_g)_{min}$	0 Nm
Global maximum value of C_p, $(C_p)_{max}$	0.4948
Value of λ corresponding to $(C_p)_{max}$, λ_*	7.54
Value of β corresponding to $(C_p)_{max}$, β_*	0 degree

Table 6: Turbine system parameters.

Step Response

Step inputs are first used to evaluate the performance of different control algorithms. Figure 18 shows the simulation results using multiple step inputs from 5 m/s to 6.5 m/s, which represents a lower range of wind speed in Region 2 operation. Since the wind power capture is determined by the turbine power coefficient, only the latter is shown. Four

controllers are compared in Fig. 18, namely the traditional TFC, the DS method using the SQP algorithm, the traditional DP and the ADP approach. It can be seen that the DP and ADP methods capture more wind energy than the DS, and the DS performs better than the TFC. As discussed earlier, a good initial guess is important to achieve a good performance for the DS approach since its uses the SQP algorithm to solve for the optimal parameters. Through several trials, a good initial guess was obtained for the DS method. Applying this good initial guess, the DS method generates the same result as the DP and ADP algorithms as shown in Fig. 19.

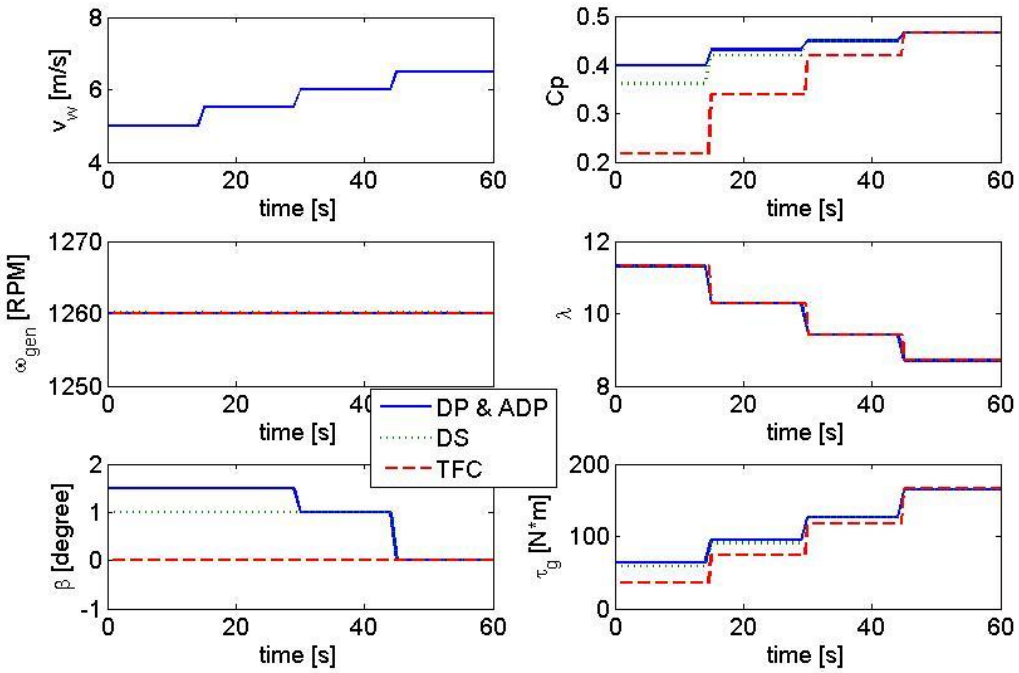

Figure 18: Performance comparison of controllers including TFC, DS, DP and ADP (low wind speed).

Since using these three control methodologies, namely DS with a good initial guess, DP and ADP can generate similar wind power, they are then defined as the numerical optimal control (NOC) method in this paper. The plot of C_p in Fig. 19 indicates that the NOC method achieves more wind energy capture than that of the traditional TFC method during the first 45 seconds. This is due to the rotor speed being limited by its lower boundary and the range of λ is between 8 to 12. According to Fig. 11, the global maximum value of C_p is not reachable within this range of λ. When λ is greater than 10, an achievable maximum value of C_p has to be used. The traditional TFC method is no longer sufficient while the NOC method finds the optimal solution through reaching the achievable maxima of C_p. After the first 45 seconds, the global maximum of C_p is attainable. The NOC method and the traditional TFC method exhibit a similar performance.

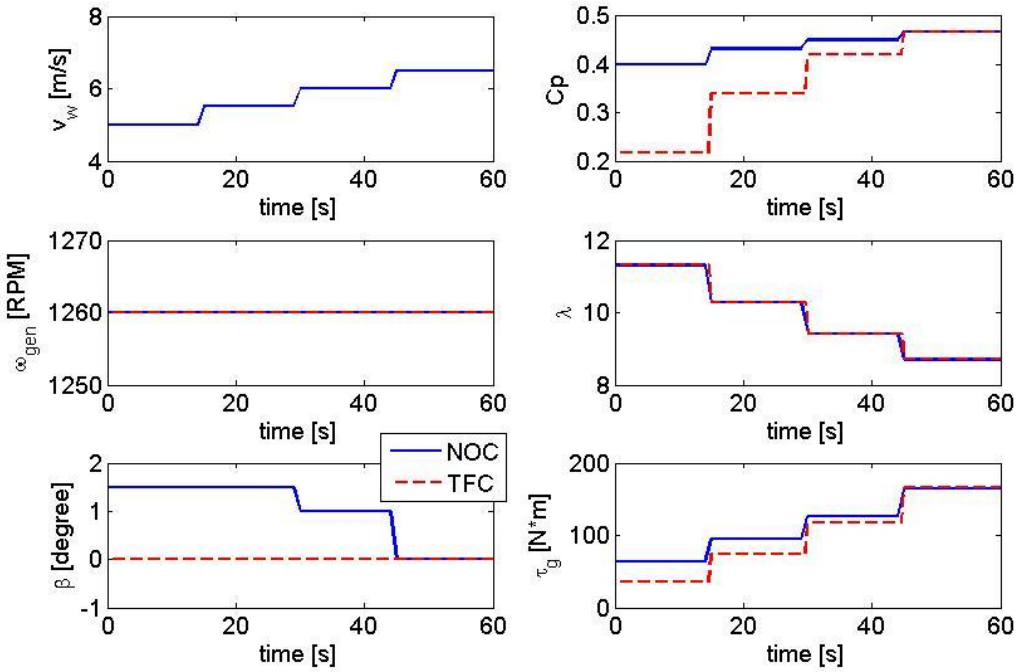

Figure 19: Performance comparison among controllers including TFC, DS with a good initial guess, DP and ADP (low wind speed).

Figure 20 shows the simulation result using multiple step inputs from 8 m/s to 11 m/s, which represents a higher range of the wind speed during the partial load region. Within this wind speed range, the range of λ given allows the turbine to reach the global maximum of C_p. Therefore, it is not necessary to find the local maxima of C_p. The NOC method and the traditional TFC approach will have similar performance. Figure 20 indicates that despite using the same maxima of C_p, the NOC method still captures more wind energy than the traditional TFC method. This is because the NOC optimizes the C_p trajectory and converges to the maximum C_p faster. Nevertheless, there is a tradeoff

between the energy capture and torque variation; under the NOC method, the torque experience more variation. More research will be conducted in the future to investigate the tradeoff between energy capture and fatigue effect.

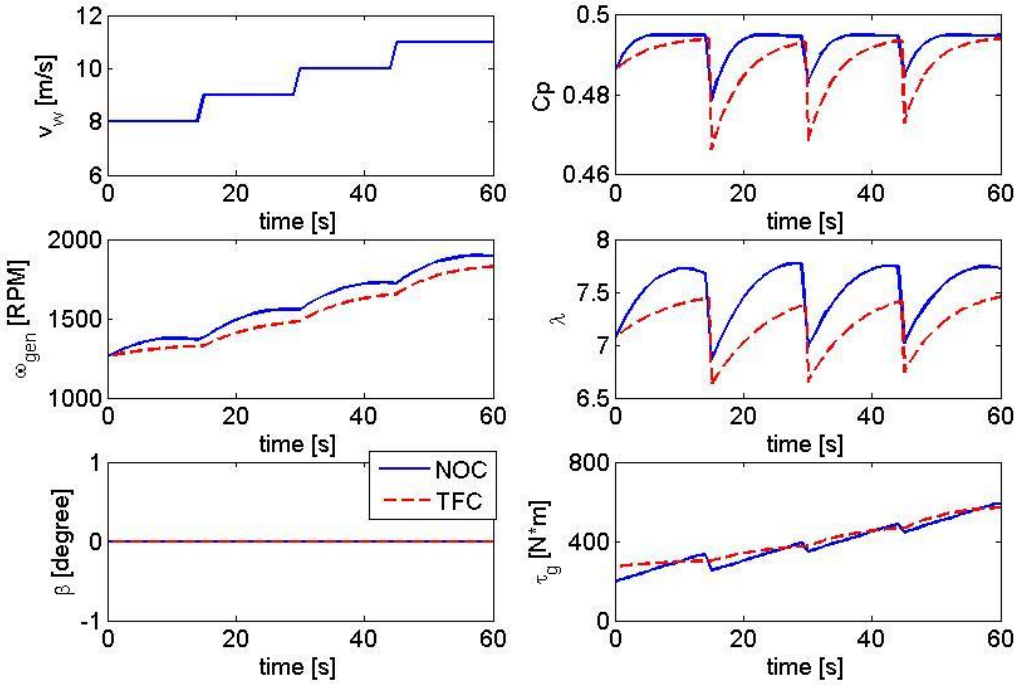

Figure 20: Performance comparison between NOC and TFC controllers (high wind speed).

Wind Speed Inputs from Wind Farm Measurements

In reality, the wind speed is continuously changing and a step input can be treated as a special case of continuous wind speed input. Wind speed data can be downloaded from the NREL official website [93] and converted to one-second interval data through the

power spectral density method [94-95].

Figure 21 shows the system performance under 1000 seconds of continuous wind speed that is between 5 m/s and 7 m/s. It is seen that the trajectory generated by the NOC method has obvious advantages over the TFC method. Due to the constraint caused by the lower limit of turbine rotor speed, the global maximum of C_p is not reachable. Similar to the first 45 seconds in Fig. 19, the NOC method can achieve the achievable maxima of C_p, thus maximize wind energy capture, while the TFC fails to do so because its feedback control is developed based on the assumption that the global maxima of C_p is always reachable. In summary, when the wind speed is low and the global maximum of C_p is not reachable, the NOC method has significant advantage over the TFC method in terms of wind energy capture by being able to find the achievable maxima of C_p. When the wind speed is relatively high and the global maximum of C_p is achievable, the advantage of the NOC method in wind energy capture diminishes.

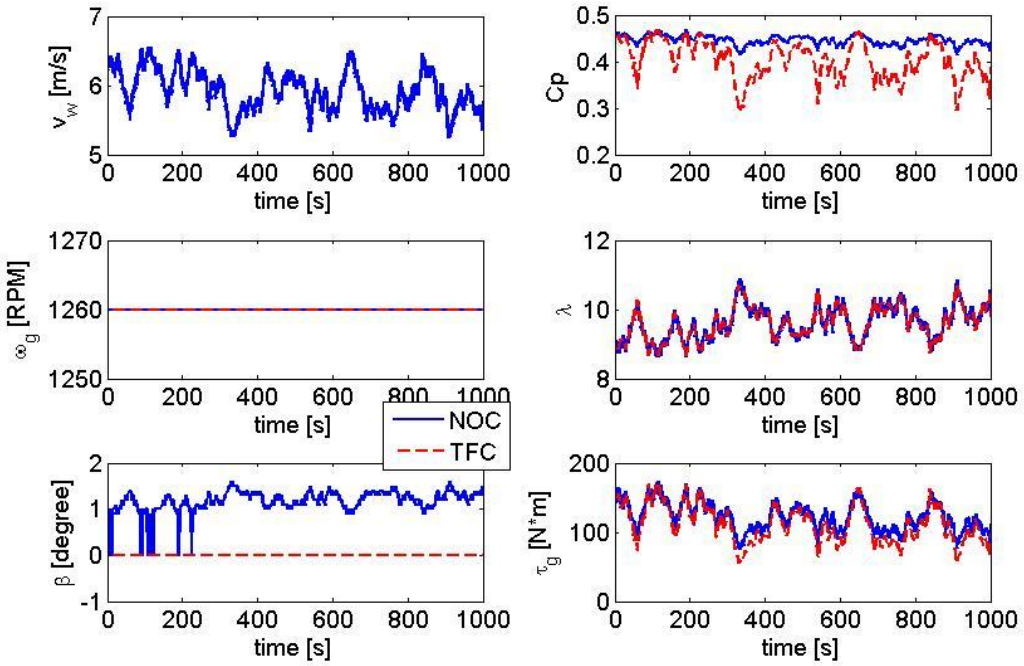

Figure 21: Performance comparison between NOC and TFC controllers under continuous wind speed input.

Computational Expense

In addition to comparing the energy capture, another important aspect of controller design is the computational time. It is desirable to design a control algorithm that maximizes the wind energy capture with minimum computational expense. In this section, the computational costs for the aforementioned control algorithms are compared based on a PC platform. Comparisons of the computational time and wind energy capture for the TFC, DS, DP, and ADP are listed in Table 7. Once a satisfactory initial guess is found for the DS method, the DS, DP and ADP will lead to the same wind energy capture. Therefore,

the NOC can represent all three algorithms with respect to wind energy capture. It is seen from Table 7 that the computational time is significantly shortened using the ADP algorithm compared to the DP. Even though the DS method uses less time to compute than the ADP algorithm. The tuning time associated with finding a good initial guess for the DS method is long. Therefore, the ADP algorithm has less overall computational expense.

Fig	Wind Profile Duration (s)	Simulation Time				Wind Energy Capture ($\times 10^6$J)		Increase over TF (%)
		TFC	DS*	DP	ADP	TFC	NOC	NOC
19	60	0.83s	32.4s	2.2h	5.2min	0.7827	0.9014	15.16
20	60	0.76s	22.4s	1.9h	2.2min	4.49519	4.5634	1.52
21	1000	0.82s	48.9s	10.2h	26.8min	14.5691	16.0576	10.22

Table 7: A comparison table on running time and wind energy capture for all of the algorithms in the 3 groups of simulations.

*It should be noted that the time spent on tuning the initial guesses of the DS method is not included in the simulation time.

Effect of C_p Uncertainty

These numerical simulations are based on the assumption of a perfectly known nonlinear model of the C_p surface, as defined in Eqns. (11) and (12). However, this model imperfectly describes real world operation, and can have up to 20% error [96]. In this section, the effect of C_p uncertainty on the system performance is explored. We assume

that C_p could be off by +/-10% of the value obtained using the perfect nonlinear model. The same wind speed input in Fig. 21 is used here.

In Fig. 22, the thicker middle solid line represents the system response using the perfect nonlinear model of C_p for the NOC method. The thinner upper and lower solid lines represent the system response when C_p is 10% greater and less than the nominal value, respectively. The dashed lines are analogous for the TFC method. Figure 22 also reveals that the proposed NOC method gives a significantly improvement in C_p over the traditional TFC method. The gain on achievable C_p proves that the NOC method still has advantages even considering the uncertainty of the power coefficient.

In addition to C_p uncertainty, other factors also influence turbine operation. For instance, the turbine fatigue is another important aspect that should be considered during control design. A comprehensive analysis will be conducted by the authors to investigate the effect of turbine control design on both wind energy capture and turbine fatigue loading in the future work.

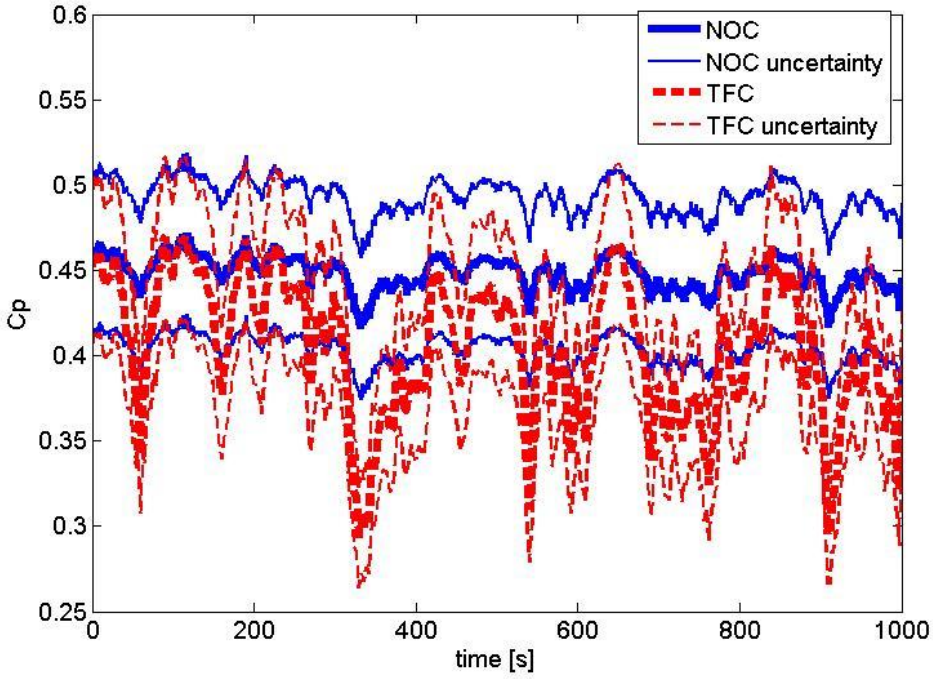

Figure 22: Comparison between C_p with and without uncertainty.

Chapter 6: *Optimal Region 2 Operation of a Wind Turbine with Time-Varying Weightings to Smooth Torque Variation*[3]

In the last chapter, we present a numerical optimal control method to maximize the wind energy of a speed constrained wind turbine during Region 2 operation and proved that it can significantly improve turbine's efficiency comparing to traditional control methods. However, like the famous Bang-Bang (on-off) optimal control [84-86], sometimes the optimal control trajectory needs to change abruptly among several control inputs in order to achieve the optimal system performance. This is not desirable for turbine generator torque control because abrupt changing in turbine generator torque will cause shear stress oscillations and result in the risk of fatigue on the turbine generator shaft [87-88]. In this chapter, we first identify the problem in the turbine generator torque trajectory when applying the numerical optimal control method to maximize the wind energy capture. Based on the identified problem, the performance index of the numerical optimal control method is modified in order to generate smoother turbine generator torque trajectory. Furthermore, the approach of time-varying weighting [89] is incorporated with the modified performance index to seek further improvement on turbine system performance. All of the control designs are validated in a simulation environment.

PROBLEM IDENTIFICATION

Simulation was conducted to identify the problem associated with the NOC method. The same turbine model with the parameters in Table 6 is used. The constraint on turbine rotor speed is removed so that the global maximum of the power coefficient is always

---

[3] ***Z. Yan***, ***D. Chen***, and ***M. Lin***, 2015,"Optimal Region 2 Operation of a Distributed Wind Turbine with Time-Varying Weightings to Smooth Torque Variation," Proceedings of 2015 American Control Conference, Chicago, IL, June 1-3.

The corresponding authors Dongmei Chen and Mengxiang Lin provided precious research advice for the above publication.

achievable, which represents a more general case of turbine's operation. Figure 23 shows the simulation result under the wind speed which first decreases from 14 m/s to 8 m/s, then increases from 8 m/s to 12 m/s. The performance index in Eqn. (31) is used to maximize the wind energy capture and the performance of the NOC method is still compared to that of the traditional TFC method. Since the wind power capture is determined by the turbine power coefficient, only the latter is shown. From Fig. 23, it is seen that when the wind speed changes from 14 m/s to 8 m/s, the turbine deviates from its steady state established at the wind speed of 14 m/s and needs to decelerate to pursue its global maximum of C_p under the wind speed of 8 m/s. Figure 23 shows that the NOC method has significant advantage over the traditional TFC method in terms of C_p before the steady state is achieved for the wind speed of 8 m/s. This is because that the NOC method generates the optimal control input trajectories in the following way

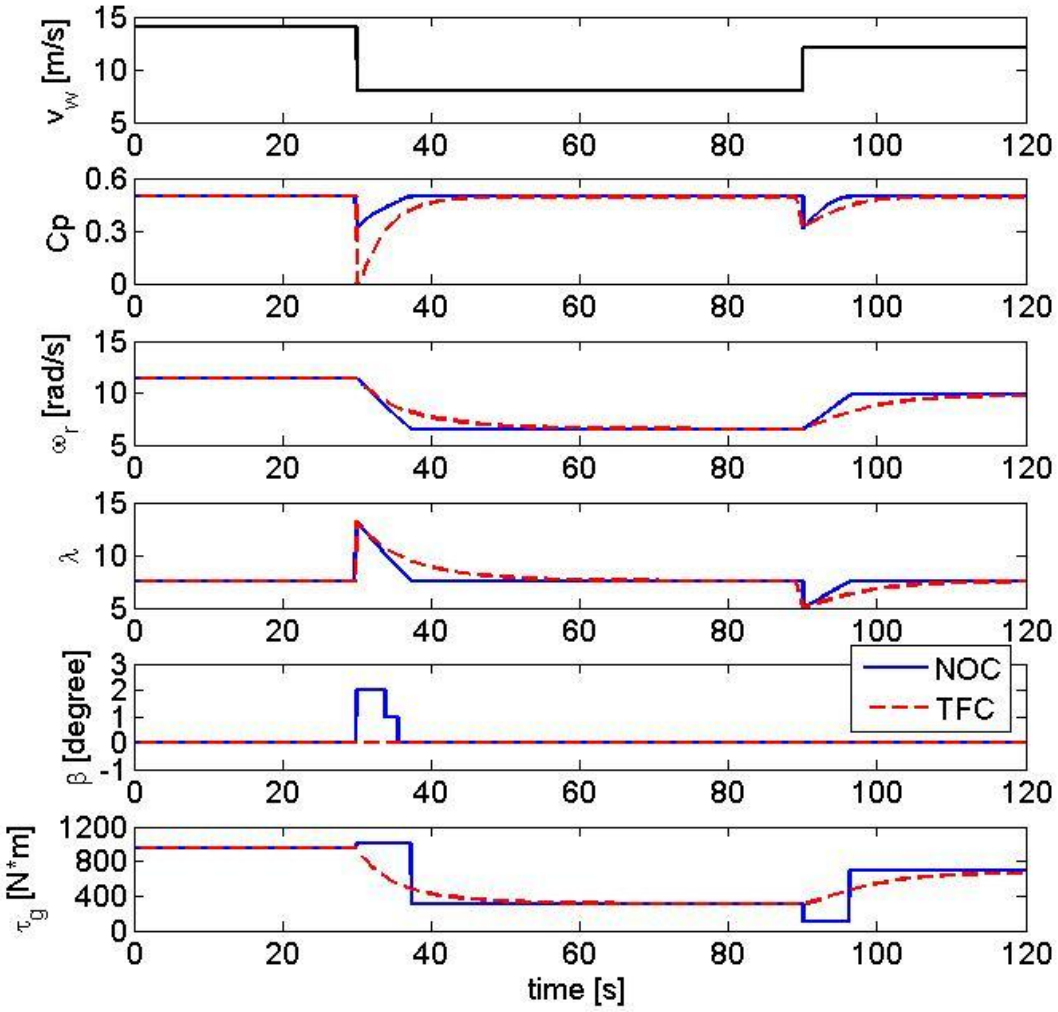

Figure 23: Performance comparison between the NOC and the TFC controllers (NOC method for maximizing wind energy capture only).

(1) The turbine rotor speed corresponding to the global maximum of C_p is found by

$$(\omega_r)_* = \frac{2v_w\lambda_*}{D_r} \tag{54}$$

where λ_* represents the corresponding λ value to the global maximum of C_p shown in Fig. 11. To achieve the global maximum of C_p under a specific wind speed, the turbine rotor speed needs to achieve the corresponding $(\omega_r)_*$. The turbine rotor angular acceleration is determined by Eqn. (7). The NOC method seeks the maximum generator torque to maximize the magnitude of the negative rotor angular acceleration until $(\omega_r)_*$ is achieved. After achieving $(\omega_r)_*$, the NOC method commands the turbine generator torque to a different value to keep the turbine rotor speed fixed as $(\omega_r)_*$, so that the turbine system can stay at its global maximum C_p value.

(2) Before the global maximum of C_p is achieved, the NOC method maximizes the wind energy capture by tuning the blade pitch angle, so that the wind turbine can pursue its achievable maximum of C_p. When the wind speed decreases from 14 m/s to 8m/s, the value of λ increases. According to Fig. 11, a 1° or 2° of β maximizes C_p when the value of λ is relatively large. On the other hand, the traditional TFC method, which is only able to track β_*, fails to do so.

Similarly, for the case of wind speed increasing from 8 m/s to 12 m/s, the turbine needs to accelerate to achieve $(\omega_r)_*$.

(1) The NOC method first seeks the minimum value of the turbine generator torque to maximize the magnitude of the positive rotor angular acceleration until the $(\omega_r)_*$ is achieved. After achieving $(\omega_r)_*$, the generator torque is changed to a specific value to keep the wind turbine operating at steady state.

(2) According to Fig. 11, the range of λ indicates that all of the achievable maximum of C_p correspond to a 0° of β. Therefore, it is not necessary to tune the blade pitch angle in this case.

Although the NOC method has significant advantage over the TFC method in terms of wind energy capture, it can be seen from Fig. 23 that the optimal generator torque

trajectory generated by the NOC method needs to switch between its boundary values and steady-state values. This kind of abrupt switching is not desirable for turbine generator torque control because it will cause shear stress oscillations and intensify the risk of fatigue on turbine generator shaft [87-88]. Hence, the smoothness of the turbine generator torque trajectory is another important factor that should be considered in our optimal control design.

OPTIMAL CONTROL DESIGN CONSIDERING TURBINE GENERATOR TORQUE VARIATION

In order to generate smoother turbine generator torque trajectory, the performance index of the NOC method needs to be modified. First, constant weightings are incorporated with the modified performance index and the tradeoff between maximizing the wind energy capture and the smoothness of the turbine generator torque trajectory is explored by varying the value of the constant weightings. Then, the approach of time-varying weightings is incorporated with the modified performance index to seek further improvements on turbine system performance.

Modified Performance Index with Constant Weightings

To mitigate the abrupt switching in the turbine generator torque trajectory, a modified performance index with an extra term which has the effect of reducing the variation in the generator torque trajectory is developed as

$$\max \quad J = \alpha \sum_{k=1}^{N-1} \frac{\int_{T_k}^{T_{k+1}} v_w^3 C_p \, dT}{\int_{T_k}^{T_{k+1}} v_w^3 \left(C_p\right)_{max} dT} - \left(1-\alpha\right) \sum_{k=1}^{N-1} \frac{\left|\left(\tau_g\right)_{k+1} - \left(\tau_g\right)_k\right|^2}{\left(\Delta \tau_g\right)_{max}^2} \tag{55}$$

where α is a constant, satisfying

$$0 \le \alpha \le 1 \tag{56}$$

and by tuning the value of α, the relative weightings associated with the two terms in the modified performance index shown in Eqn. (55) can be tuned to satisfy different control requirements. For the denominators, $(C_p)_{max}$ is the global maximum value of C_p shown in Fig. 11 and $(\Delta\tau_g)_{max}$ represents the maximum variation in turbine generator torque, which can be determined using the torque constraint in Eqn. (36)

$$\left(\Delta\tau_g\right)_{max} = \left(\tau_g\right)_{max} - \left(\tau_g\right)_{min} \tag{57}$$

The first term in Eqn. (55) still has the effect of maximizing wind energy capture, while the second term together with the minus sign in front of it has the effect of reducing the variation in the turbine generator torque trajectory, namely making the turbine generator torque trajectory smoother. By adding the denominators, the magnitudes of the two terms are of the same scale and the performance of the system can be further tuned by tuning the value of α. Consider two extreme cases

$$\begin{aligned} &1) \quad \alpha = 1 \quad \text{and} \quad 1-\alpha = 0 \\ &2) \quad \alpha = 0 \quad \text{and} \quad 1-\alpha = 1 \end{aligned} \tag{58}$$

For case 1), the term associated with reducing the torque variation in Eqn. (55) vanishes and the only term remaining is the term associated with maximizing the wind energy capture. This corresponds to the extreme case that the only control objective is to maximize the wind energy capture and the performance index in Eqn. (55) becomes equivalent to the original performance index in Eqn. (31). Therefore, the optimal control input trajectories generated by the NOC method and the resulted system performance will be the same as that shown in Fig. 23.

For case 2), the term associated with maximizing the wind energy capture in Eqn. (55) vanishes and the only term remaining is the term associated with reducing the torque variation. This corresponds to the extreme case that the only control objective is to minimize the variation in the turbine generator torque trajectory. In this case, the NOC method takes no account of the wind energy capture and the turbine generator torque trajectory generated by it will be at steady state with zero variation. The steady-state value of the turbine generator torque trajectory will only depend on its initial condition.

For all the other values of α satisfying $0 < \alpha < 1$, the resulted turbine system performance using the NOC method with the modified performance in Eqn. (55) will depend on the value of α. The more the value of α is close to 1, the more wind energy capture can be achieved. The more the value of α is close to 0, the smoother the turbine generator torque trajectory can be generated. Therefore, there is a tradeoff between maximizing the wind energy capture and the smoothness of the turbine generator torque trajectory. A suitable value of α needs to be chosen to fulfill any specific design requirement.

Simulation Results Using Constant Weightings

Simulations were conducted to evaluate the performance of the NOC method using the modified performance index defined in Eqn. (55) with different constant weightings. Discrete values of 0.3, 0.5 and 0.7 were chosen for α to demonstrate our methodology. For comparison purpose, the same wind speed input in Fig. 23 is used and the results are shown in two separate figures. Comparisons of the resulted wind energy capture for different values of α are shown in Table 8.

Figure 24 shows the simulation result when the wind speed first decreases from 14 m/s to 8 m/s. In the legend, `Original NOC' represents the result generated by the NOC

method using the original performance index in Eqn. (31) and the others represent the results generated by the NOC method using the modified performance index in Eqn. (55) with the different constant weightings. From Fig. 24, it can be seen that as the value of α decreases, the weighting associated with reducing the variation in the turbine generator torque trajectory increases and the slope of the turbine generator torque trajectory to switch from its upper boundary to the steady-state value becomes more level. Therefore, smoother turbine generator torque trajectories are generated as the value of α decreases. On the other hand, as the value of α decreases, the weighting associated with maximizing the wind energy capture also decreases and it takes longer time for the power coefficient to achieve its maximum value. Therefore, there is more sacrifice in wind energy capture as the value of α decreases and this result can be verified using the data shown in Table 8.

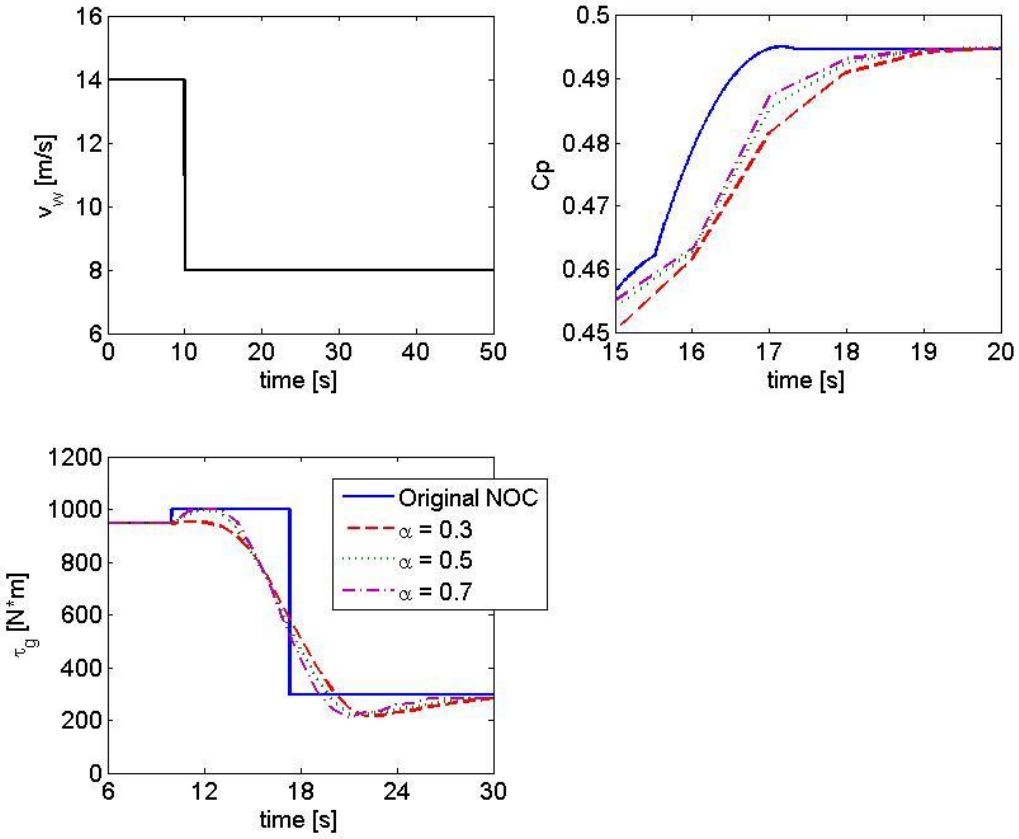

Figure 24: Performance comparison among the original NOC method and the NOC method using the modified performance index with different constant weightings. (Wind speed decreases from 14 m/s to 8 m/s.).

Figure 25 shows the simulation result when the wind speed increases from 8 m/s to 12 m/s. Similarly to Fig. 24, we can also see that as the value of α decreases, the slope of the turbine generator torque trajectory to switch from its lower boundary to the steady state becomes more level. Therefore, as the value of α decreases, the turbine generator torque trajectory also becomes smoother. On the other hand, there is also more sacrifice in wind energy capture as the value of α decreases since it takes longer time for the power

coefficient to achieve its maximum value. This result can also be verified using the data shown in Table 8.

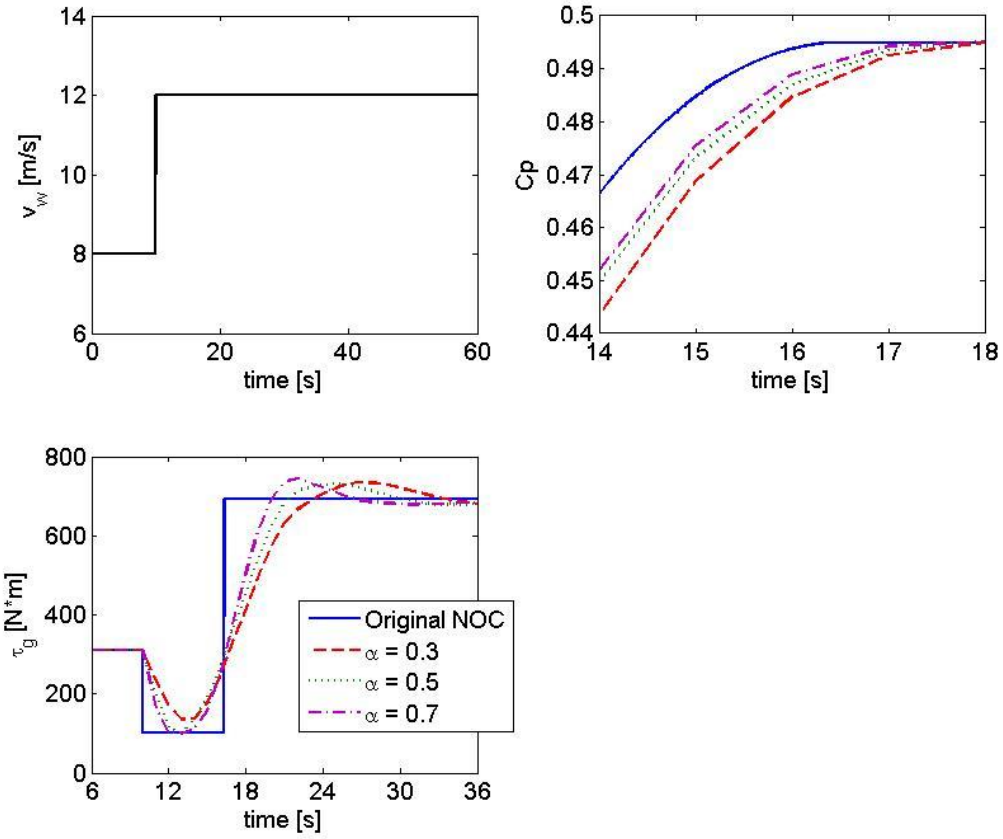

Figure 25: Performance comparison among the original NOC method and the NOC method using the modified performance index with different constant weightings. (Wind speed increases from 8 m/s to 12 m/s.).

The simulation results in Figs. 24 and 25 reveal that the NOC method using the modified performance index in Eqn. (55) with constant weightings is able to generate smoother turbine generator torque trajectories comparing to the NOC method using the

original performance index in Eqn. (31) whose only control objective is to maximize the wind energy capture. The simulation results together with the wind energy capture data in Table 8 also reveal that there is a tradeoff between maximizing the wind energy capture and the smoothness of the turbine generator torque trajectory. In order to generate smoother turbine generator torque trajectories, there needs to be sacrifice in wind energy capture.

Fig	Time (s)	Wind Energy Capture ($\times 10^6$ J)					Energy Drop to NOC (%)			
		Original NOC	$\alpha = 0.3$	$\alpha = 0.5$	$\alpha = 0.7$	TFC	$\alpha = 0.3$	$\alpha = 0.5$	$\alpha = 0.7$	TFC
24	50	4.0158	3.9804	3.9998	4.0007	3.9596	0.88	0.40	0.38	1.4
25	50	6.1739	6.1348	6.1437	6.1482	6.1294	0.63	0.49	0.42	0.72

Table 8: A comparison table on wind energy capture for different values of α.

Modified Performance Index with Time-Varying Weightings

For the modified performance index defined in Eqn. (55), the values of the constant weightings are tuned to explore the tradeoff between maximizing the wind energy capture and the smoothness of the turbine generator torque trajectory. In this section, we present the utilization of time-varying weightings instead of constant weightings in the modified performance index to seek further improvement on turbine system performance. The approach of time-varying weighting has been applied to optimal servo control to achieve high seek/settle performance without compromising the targeted seek time in hard disk drives and is more effective to minimize the settling vibration induced by the actuator seek

profile compared to previous optimization approaches in the literature [89]. The same concept can be adopted in our optimal control design, aiming for further improvement on the smoothness of the turbine generator torque trajectory without significant sacrifice in the wind energy capture.

The modified performance index with time-varying weightings is defined as follows

$$\max \quad J = \alpha(T)\sum_{k=1}^{N-1}\frac{\int_{T_k}^{T_{k+1}} v_w^3 C_p dT}{\int_{T_k}^{T_{k+1}} v_w^3 \left(C_p\right)_{max} dT} - \left[1-\alpha(T)\right]\sum_{k=1}^{N-1}\frac{\left|\left(\tau_g\right)_{k+1}-\left(\tau_g\right)_k\right|^2}{\left(\Delta\tau_g\right)_{max}^2} \tag{59}$$

where

$$0 \le \alpha(T) \le 1 \tag{60}$$

is a function of the normalized time.

By choosing $\alpha(T)$ to be different type of functions, different system behaviors can be achieved. From the simulation results of the NOC method using the original performance index in Eqn. (31), it is found that a wind turbine will eventually achieve its global maximum power coefficient and steady state every time the wind speed changes. It is the dynamics before achieving the steady state that determines the total wind energy capture. Therefore, the weighting associated with maximizing the wind energy capture in the modified performance index plays the dominate role in improving turbine's efficiency. It is also found that, as time increases, the weighting associated with reducing the variation in the turbine generator torque trajectory should be increased in order to decrease the rate

of change when the turbine generator torque needs to switch from its boundary value to the steady-state value. Finally, when the steady state is achieved, there should be no variation in the turbine generator torque trajectory. Hence, the following properties need to be satisfied by $\alpha(T)$

- $\alpha(0) = 1$;
- $\alpha(\infty) \to 0$;
- $\alpha(T)$ keeps decreasing as T increases.

There are various functions that are suitable to achieve the above objective. The following are some common examples

$$\alpha_1(T) = \frac{1}{(T/T_{scale})^n + 1}, \quad n = 1, 2, 3, \ldots$$
$$\alpha_2(T) = \frac{1}{e^{T/T_{scale}}} \tag{61}$$

Different functions have different rate of decreasing and can be chosen to fulfill different control design requirements. Fine adjustment on the rate of decreasing of $\alpha(T)$ can also be achieved by tuning the scaling factor T_{scale}, without changing the form of the function. The integration of time-varying weightings into the modified performance index further enhances the flexibility of the proposed optimal control design methodology. By applying the time-varying weightings to the modified performance index, the NOC method is able to focus on different control objectives during different stages of turbine's operation and makes it possible to seek further improvement on the smoothness of the turbine generator torque trajectory without significant sacrifice in the wind energy capture.

Simulation Results Using Time-Varying Weightings

Simulations were conducted to explore the turbine system performance using the modified performance index with time-varying weightings and the results are compared to those generated using constant weightings and the original performance index. For comparison purpose, the same wind speed inputs in Figs. 24 and 25 are used. The constant weighting of $\alpha = 0.5$ and the time-varying weighting which has the form of $\alpha_1(T)$ with $n = 1$ in Eqn. (61) are chosen for the subsequent comparisons to demonstrate our methodology. The resulted wind energy capture of the aforementioned methods is shown in Table 9.

Figure 26 shows the simulation result when the wind speed decreases from 14 m/s to 8 m/s. In the legend, `Original NOC' represents the result generated by the NOC method using the original performance index in Eqn. (31); `NOC with CW' represents the result generated by the NOC method using the modified performance index in Eqn. (55) with the constant weighting of 0.5; `NOC with TW' represents the result generated by the NOC method using the modified performance index in Eqn. (59) with the time-varying weighting which has the form of $\alpha_1(T)$ with $n = 1$ and $T_{scale} = 15$ in Eqn. (61). From Fig. 26, it is seen that the C_p trajectory generated by the NOC method using the modified performance index with time-varying weighting achieves the maximum value faster than that with constant weighting. Therefore, more wind energy is captured using the time-varying weighting than the constant weighting before the maximum power coefficient is achieved. Even though there is some loss in wind energy capture after the maximum power coefficient is achieved due to using a smoother generator torque trajectory, it can be seen from Table 9 that the time-varying weighting still has slight advantage in terms of the resulted wind energy capture over the constant weighting. On the other hand, it is seen that the slope of the turbine torque trajectory to switch from its upper boundary to the minimum

value is significantly more level using the time-varying weighting compared to that of constant weighting. Therefore, the turbine torque trajectory generated using time-varying weightings is smoother than that generated using constant weighting.

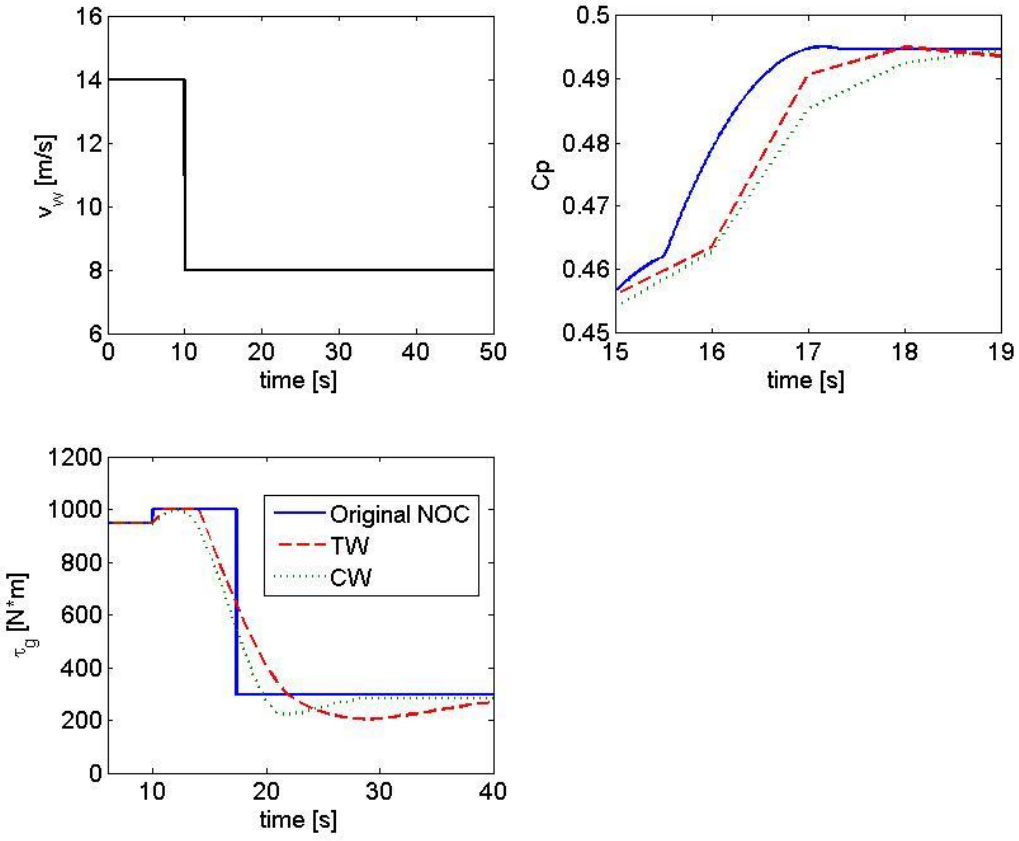

Figure 26: Performance comparison among the original NOC method, the NOC method using modified performance index with time-varying and constant weightings. (Wind speed decreases from 14 m/s to 8 m/s.).

Figure 27 shows the simulation result when the wind speed increases from 8 m/s to 12 m/s. Similarly to the previous case, the time-varying weighting still enables more wind energy capture by making the power coefficient achieve the maximum value faster than

the constant weighting. On the other hand, the slope of the turbine torque trajectory to switch from its lower boundary to the maximum value is also significantly more level using the time-varying weightings compared to that of constant weightings. Therefore, the turbine torque trajectory generated using time-varying weightings is still smoother than that generated using constant weightings.

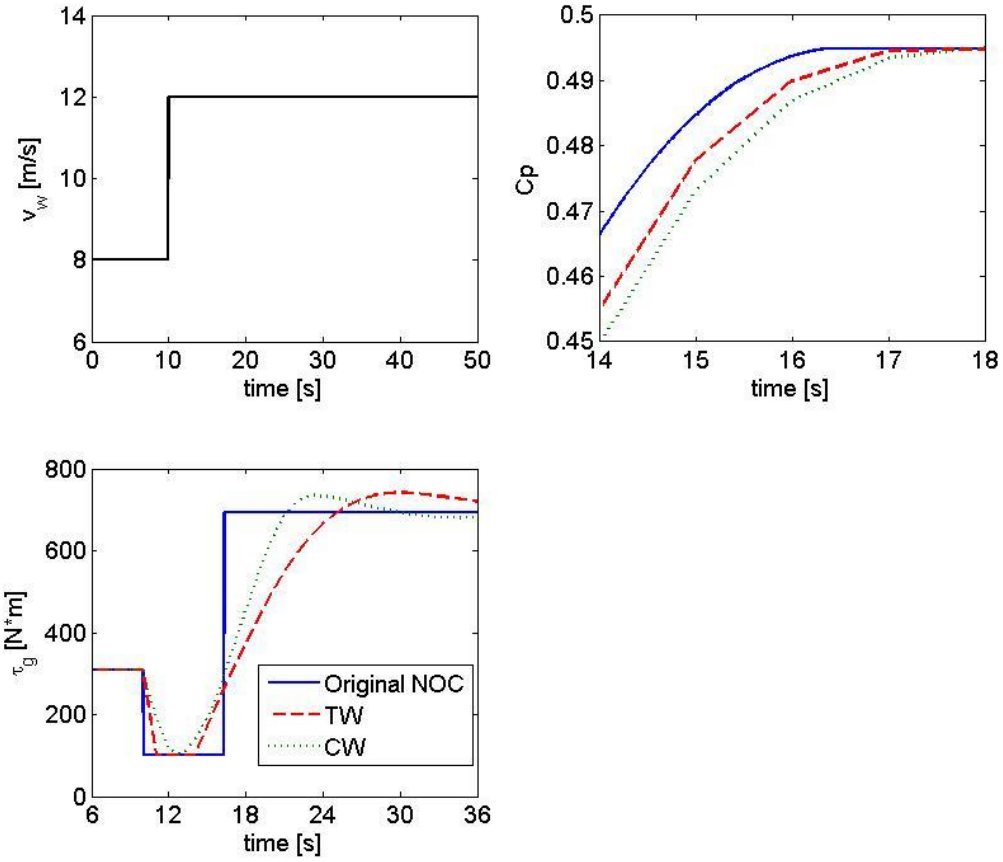

Figure 27: Performance comparison among the original NOC method, the NOC method using modified performance index with time-varying and constant weightings. (Wind speed increases from 8 m/s to 12 m/s.)

Fig	Time (s)	Wind Energy Capture ($\times 10^6$ J)			Energy Drop to NOC (%)	
		Original NOC	TW	CW ($\alpha = 0.5$)	TW	CW ($\alpha = 0.5$)
26	50	4.0158	4.0001	3.9998	0.39	0.40
27	50	6.1739	6.1443	6.1437	0.48	0.49

Table 9: A comparison table between the original NOC method, the NOC method with modified performance index with constant and time-varying weightings.

The simulation results in Figs. 26 and 27 reveal that by applying time-varying weighting to the modified performance index of the NOC method, the turbine system performance can be further improved. Comparing to constant weighting, the time-varying weighting enables more wind energy capture while still generates smoother generator turbine trajectory. The integration of time-varying weighting to the optimal control design leads to an overall more efficient wind turbine system.

Chapter 7: *Maximizing Wind Energy Capture for a Switched Wind Turbine System*

For the last two chapters, our research focuses improving turbine's performance during Region 2 operation. In this chapter, operation modes of the wind turbine system are defined in a different way. Depending on the load power demand and the wind speed, the wind turbine's operation may switch between two modes: a multi-input-single-output (MISO) mode and a single-input-single-output (SISO) mode. In this chapter, we present an optimal control framework to maximize the wind energy capture of a wind turbine system when switching is involved in its operation. The effectiveness of the optimal control design is validated through comparing to the traditional control methods in a simulation environment. The performance of the turbine system is explored under different wind speed inputs and load power demands.

OPERATION MODES

Depending on the value of the wind speed and the load power demand, the wind turbine operates in one of the following two operation modes [34]:

(1) MISO (Multi-Input-Single-Output) Mode: When the captured wind power is not sufficient to meet the load power, both the blade pitch angle and the turbine generator torque are used to control the turbine speed in order to track the maximum power coefficient, thus maximizing the wind power capture. This is the MISO mode. In the MISO mode, the turbine's dynamic equation remains the same as Eqn. (7).

(2) SISO (Single-Input-Single-Output) Mode: When the turbine can generate more power than the load power, the turbine generator output power is limited to be the load power. This is the SISO mode. In SISO mode, we have

$$P_g = \tau_g \omega_r G_r = P_{load} \tag{62}$$

which yields

$$\tau_g = \frac{P_{load}}{\omega_r G_r} \tag{63}$$

By substituting Eqn. (63) into Eqn. (7), the turbine's dynamic equation under SISO mode can be derived

$$\dot{\omega}_r = \frac{1}{J_r}\left(\frac{\pi}{8} D_r^2 \rho_{air} C_p \frac{v_w^3}{\omega_r} - \frac{P_{load}}{\omega_r}\right) \tag{64}$$

Equation (64) indicates that the blade pitch angle is the only control input under SISO mode.

CONTROL DESIGN

We first recapture the traditional control methods for each of the corresponding operation mode, which are widely used in industry because of their good performance and simple implementation. The performance of the traditional methods will be set as a benchmark for further comparison to our optimal control design. Then, the details about our optimal control design will be introduced.

Traditional Methods

Traditional control methods are designed to maximize turbine's efficiency for each of the specific operation mode [34]. For the MISO mode, the control objective is to maximize the wind energy capture and this can be realized by tracking the maximum value

of the aerodynamic power coefficient. Therefore, the traditional control method for the MISO mode is the same as the traditional torque feedback control (TFC) method, which was introduced in Chapter 5, Eqns. (13) through (16).

For the SISO mode, β is the only control input and the control objective is to maintain the turbine generator power as the load power. The following PI control law is proposed to drive the turbine generator output power towards the load power [34]

$$\beta = K_p\left(P_g - P_{load}\right) + K_i\int\left(P_g - P_{load}\right)dt \tag{65}$$

Although the traditional methods work well for each of the specific mode, it may not guarantee the maximum overall wind energy capture when switching is involved in turbine's operation. The reason is that the traditional methods are designed to realize the control objectives for each of the corresponding mode, but not capable of maximizing the overall wind energy capture over a specific time period, during which several switchings may be involved. Therefore, it is necessary to develop an optimal controller which is capable of maximizing the overall wind energy capture of a wind turbine over a specific period of time when switching is involved in turbine's operation.

Optimal Control Design

In our research, numerical optimal control (NOC) method is applied to the switched wind turbine system to maximize the overall wind energy capture. The procedures of applying the NOC method to the switched wind turbine system is basically the same as that introduced in Chapter 5. The optimal control problem is first converted into a parameter optimization problem and then numerical optimization techniques are applied to solve for the optimal parameters. Based on the optimal parameters, the optimal control input

trajectories can be determined through interpolation. Once the optimal control input trajectories are determined, the optimal state output trajectories can be determined through integrating the state equations of the system. The difference is that the form of the state equation of the switched system depends on its operation mode. If the turbine's operation is in the MISO mode, the state equation of the system will be the one shown in Eqn. (7). If the turbine's operation is in the SISO mode, the state equation of the system will be the one shown in Eqn. (64). The proposed optimal controller will decide the timing for the turbine to switch between the operation modes in order to maximize the overall wind energy capture throughout turbine's operation period. After the optimal control input trajectories are determined using the numerical optimal controller, the optimal state output trajectories can be generated by integrating the either Eqn. (7) or Eqn. (64) depending on its operation mode.

SIMULATION RESULTS AND ANALYSIS

Simulations were conducted on a switched wind turbine system to evaluate the performance of the proposed NOC method with respect to wind energy capture. The same wind turbine model for the last two chapters is used and the simulation parameters are provided in Table 6. The performance of the proposed NOC method is compared to that of the traditional methods. Wind speed in the forms of a step input and a continuous input are used to evaluate the system performance. Turbine system performance under constant and varying load power demands are also investigated.

Step Input

Step inputs are first used to evaluate the performance of the proposed NOC method. Figure 28 shows the simulation result under the wind speed which steps down from 8 m/s to 6 m/s. In the legend, `NOC' stands for the numerical optimal control; `TM' stands for

the traditional methods. The load power demand is kept constant as 40 kW. When the wind speed drops from 8 m/s to 6 m/s, the maximum captured wind power is no longer sufficient to meet the load power and the turbine's operation needs to switch from the SISO mode to the MISO mode. It is seen from Fig. 28 that the turbine deviates from its steady state established at the wind speed of 8 m/s and needs to decelerate to pursue its global maximum of C_p under the wind speed of 6 m/s. Figure 28 shows that the NOC method has significant advantage over the traditional method in terms of C_p and captured wind power before the steady state under the wind speed of 6 m/s is achieved. This is because the NOC method generates the optimal control input trajectories in the following way

1) The turbine rotor speed corresponding to the global maximum of C_p is found using Eqn. (54). To achieve the global maximum of C_p under a specific wind speed, the turbine rotor speed needs to achieve the corresponding $(\omega_r)_*$. Under the MISO mode, the turbine rotor angular acceleration is determined by Eqn. (7). The NOC method seeks the maximum generator torque to maximize the magnitude of the negative rotor angular acceleration until $(\omega_r)_*$ is achieved. Since the turbine generator output power cannot exceed the load power, the maximum turbine generator torque is determined by

$$\left(\tau_g\right)_{max} = \frac{P_{load}}{\omega_r G_r} \tag{66}$$

   After achieving $(\omega_r)_*$, the NOC method commands the turbine generator torque to a different value to keep the turbine rotor speed fixed as $(\omega_r)_*$, so that the turbine system can stay at its global maximum C_p value.

2) Before the global maximum of C_p is achieved, the NOC method maximizes the wind energy capture by tuning the blade pitch angle, so that the wind turbine can pursue its

achievable maximum of C_p. Due to the step down of the wind speed from 8 m/s to 6 m/s, the value of λ becomes larger than λ_* and falls into the range where the maximum achievable C_p is generated by a 2° of β in Fig. 11. Then, as the turbine rotor speed decreases, the value of λ also decreases and the NOC method further tunes β to be 1° or 0° to make the turbine pursue its achievable maximum of C_p.

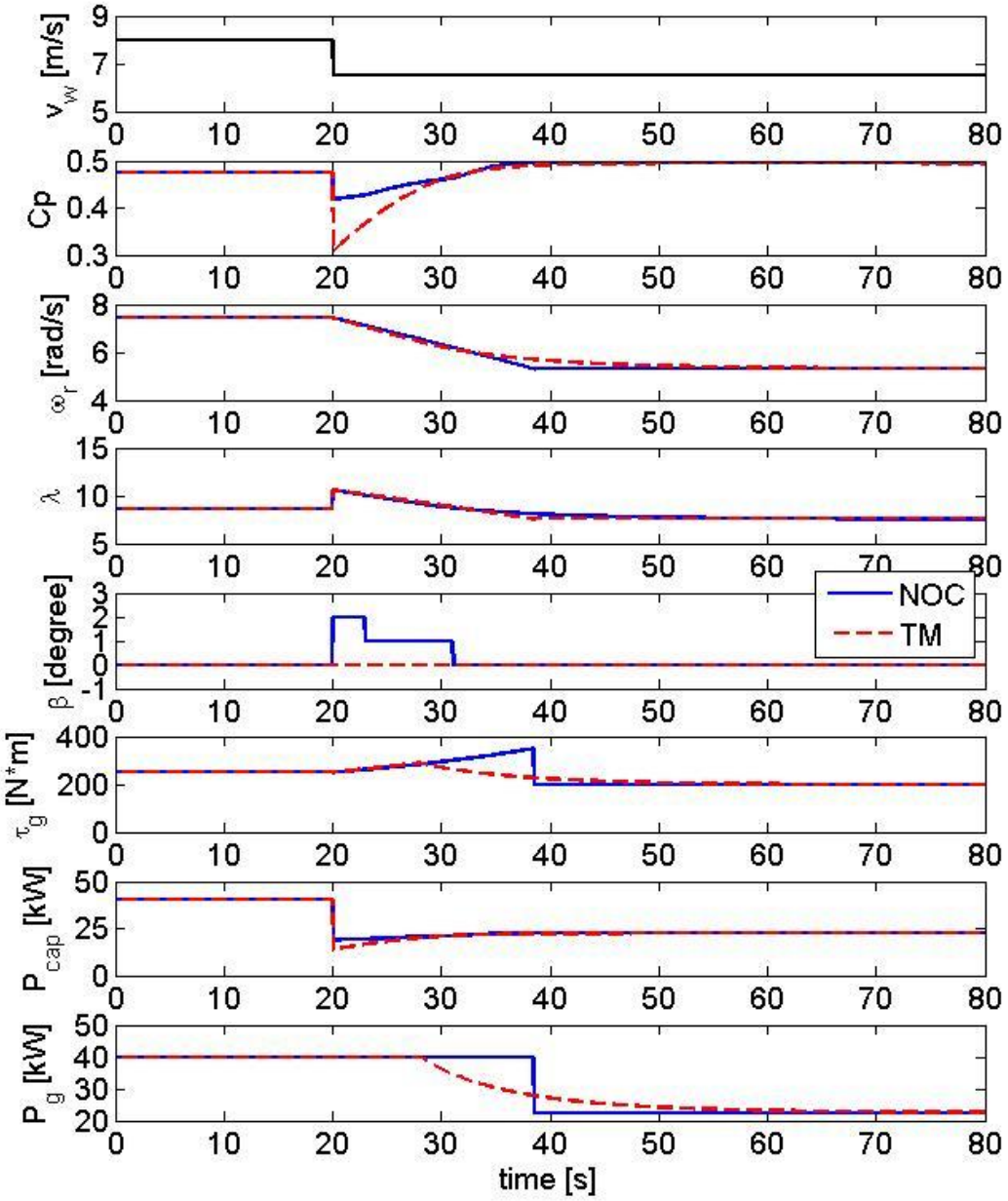

Figure 28: Performance comparison between the NOC method and the traditional methods under the wind speed input which steps down from 8 m/s to 6 m/s.

Figure 29 shows the simulation result under the wind speed which steps up from 7.5 m/s to 12 m/s. When the wind speed increases from 7.5 m/s to 12 m/s, the maximum wind energy capture becomes sufficient to meet the load power and the turbine's operation needs to switch form the MISO mode to the SISO mode. In this case, the turbine deviates from its steady state established at the wind speed of 7.5 m/s and needs to accelerate to pursue its global maximum of C_p under the wind speed of 12 m/s. Figure 29 shows that the NOC method still has significant advantage over the traditional method in terms of C_p and captured wind power. This is because of the following reasons:

1) When the turbine is able to generate more power than the load power, the NOC method and the traditional methods both make the turbine maintain its generator output power as the load power. This is realized by setting the turbine generator torque as Eqn. (63) and will make the turbine accelerate to achieve a new steady-state.
2) As the rotor speed increases, the value of λ also increases. When the value of λ falls into the range where the achievable maximum of C_p is no longer generated by a 0° of β, the NOC method is able to tune the blade pitch angle to pursue the achievable maximum of C_p. From Fig. 27, it is seen that the NOC method tunes β from 0° to 1° and 2° in order to make the turbine pursue its achievable maximum of C_p.

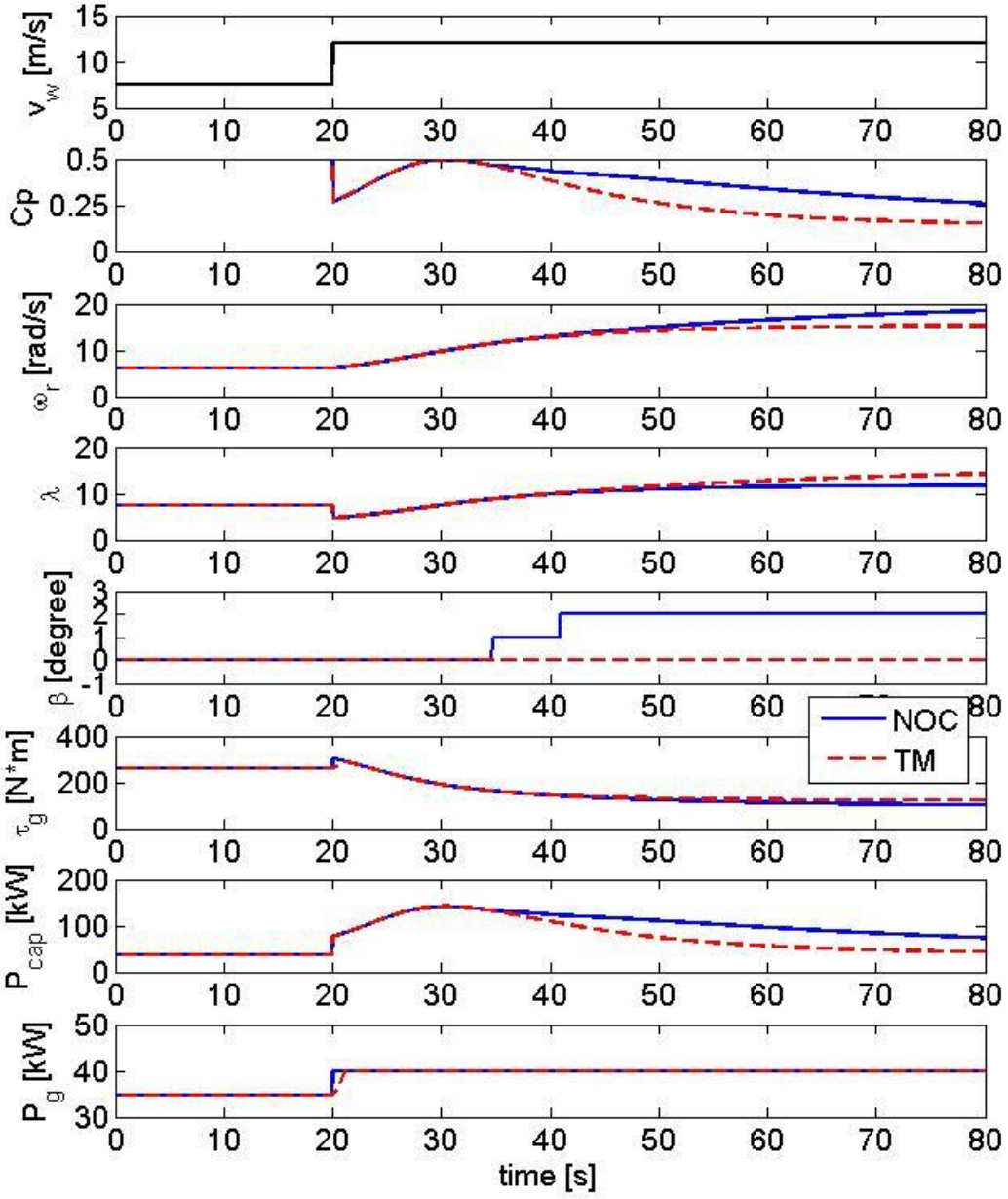

Figure 29: Performance comparison between the NOC method and the traditional methods under the wind speed input which steps up from 7.5 m/s to 12 m/s.

From the simulation results under different step inputs, it is revealed that the NOC method has significant advantage over the traditional method in terms of C_p and captured wind power by generating the optimal control input trajectories.

Real Wind Speed Input

Wind speed data from real wind farm measurement is also used to validate our optimal control methodology on switched wind turbine system. Wind speed data was downloaded from the NREL official website [93] and converted to data with different frequencies through the power spectral density method [94-95]. For our simulations, the time step is set to be 0.05 seconds.

Figure 30 shows the simulation result under real wind speed input which is higher during the first 400 seconds than the next 200 seconds. The drop in wind speed causes the turbine's operation to switch from the SISO mode to the MISO mode. From Fig. 30, it is seen that the NOC method has significant advantage over the traditional method in terms of C_p and captured wind power. This is because

1) When operating in the SISO mode, both the NOC method and the traditional method maintain the turbine generator output power as the load power by setting the turbine generator torque as defined in Eqn. (63). The only factor that changes the dynamics of the turbine is the blade pitch angle. Due to the variation in wind speed and rotor speed, the value of λ varies and may fall into the range where the global maximum of C_p is no longer achievable. In this case, the NOC method enables higher C_p and captured wind power by tuning β to make the turbine pursue its achievable maxima of C_p.
2) When operating in the MISO mode, the turbine generator torque and the blade pitch angle are controlled at the same time to maximize the wind energy capture. Both the methods will make the turbine decelerate to pursue its global maximum of C_p. Due to

the turbine dynamics to maximize the wind energy capture during the SISO mode, the rotor speed of the NOC method is higher than the traditional method before switching to the MISO mode and this makes it take longer time for the rotor speed of the NOC method to achieve $(\omega_r)_*$ defined in Eqn. (53) than the traditional method. The slower convergence of the rotor speed to $(\omega_r)_*$ causes the NOC method to capture lower wind power than the traditional method during the initial stage of the MISO mode. This part of deficiency in captured wind power is not significant because the NOC method generates the optimal control input trajectories so that it only takes a short amount of time for the turbine to achieve its global maximum of $(\omega_r)_*$ and steady state. Therefore, the overall wind energy capture through the turbine's operation can still be improved significantly by applying the NOC method over the traditional method.

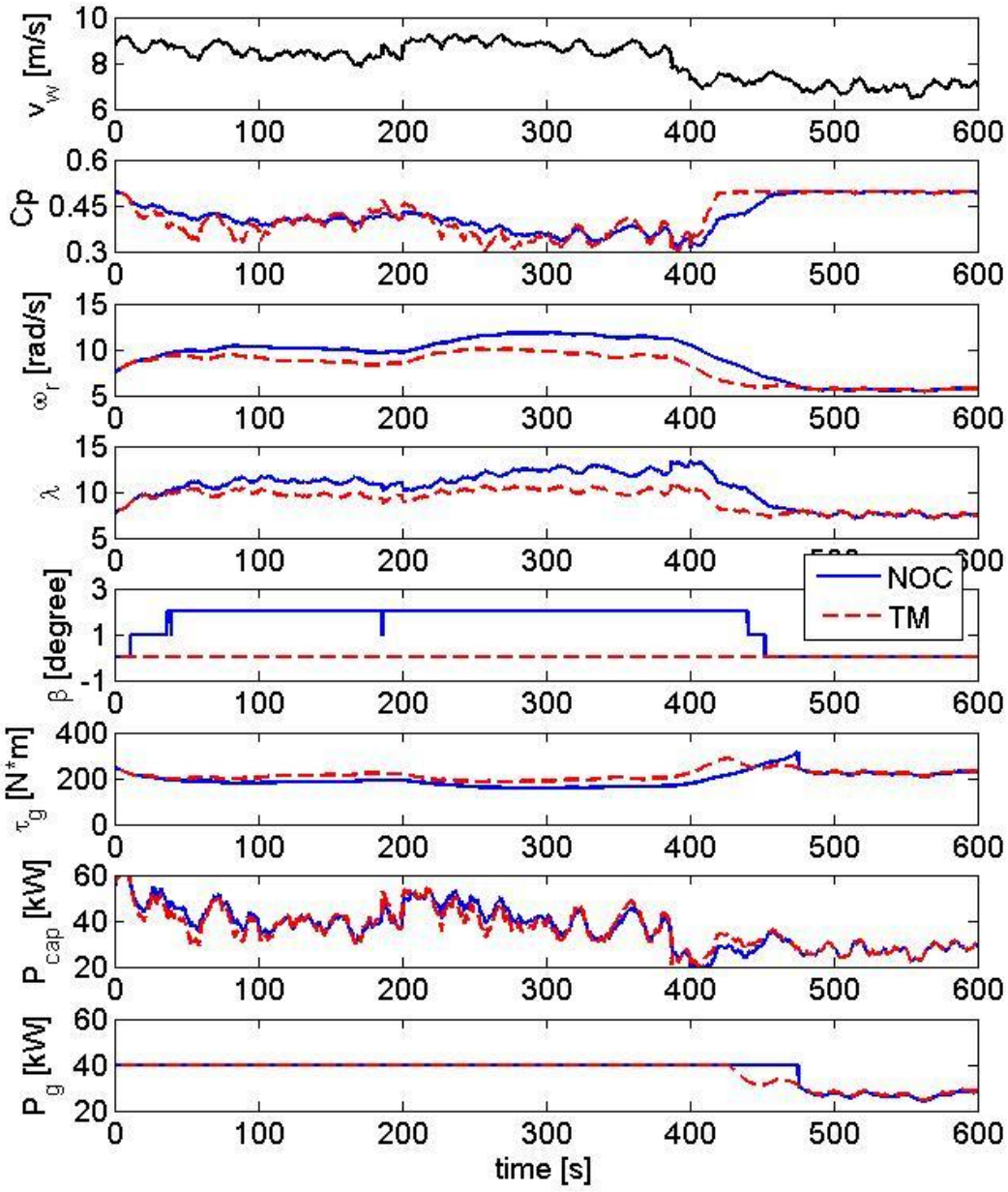

Figure 30: Performance comparison between the NOC method and the traditional methods under real wind speed input which decreases.

Figure 31 shows another group of simulation result under real wind speed input. In this case, the increase in the wind speed leads to the increase in the turbine generator output power, which finally causes the turbine's operation to switch from the MISO mode to the SISO mode. From Fig. 31, it can be seen that the NOC method still has significant advantage over the traditional method in terms of C_p and captured wind power. The reason is the following

1) During the first 200 seconds of the simulation, the wind speed is low and the turbine's operation is in the MISO mode. Both the NOC method and the traditional method tune τ_g and β to maintain C_p at its global maximum value to maximize the wind energy capture. Since the turbine's operation is already close to its global maximum value of C_p, the difference between the NOC method and the traditional method is insignificant.
2) Then, the increase in wind speed causes the turbine's operation to switch from the MISO mode to the SISO mode. Both the NOC method and the traditional method need to maintain the turbine generator output power as the load power by setting the turbine generator torque as defined in Eqn. (63) and this causes the turbine to accelerate during the SISO mode. Due to the increase in the rotor speed, the value of λ also increases and causes C_p to deviate from its global maximum value. The NOC method enables higher wind energy capture than the traditional method by generating the optimal β trajectory which makes the turbine pursue its achievable maxima of C_p.

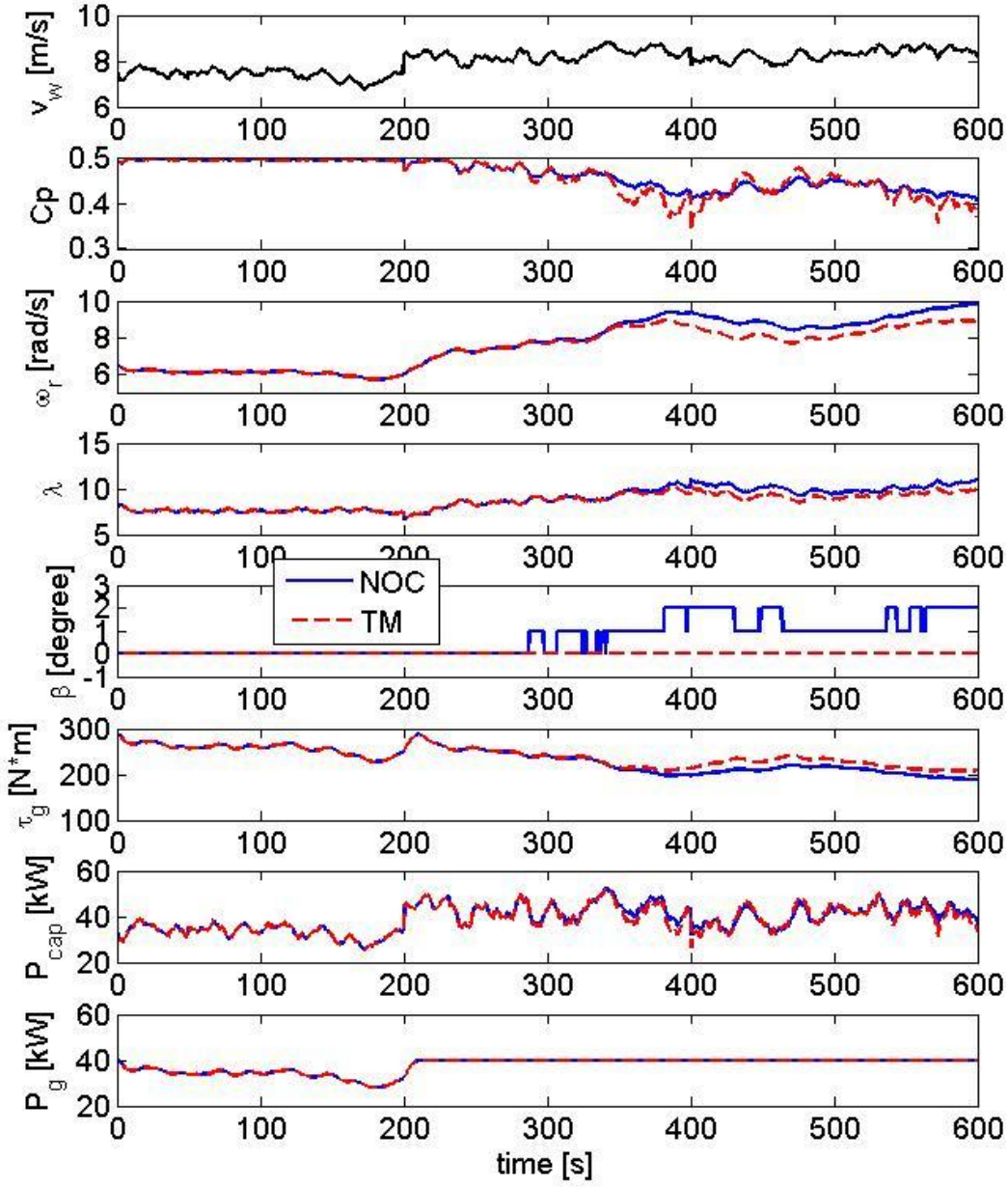

Figure 31: Performance comparison between the NOC method and the traditional methods under real wind speed input which increases.

From the simulation results under real wind speed inputs, it is revealed that the NOC method still enables the turbine to capture more wind energy compared to that of the traditional methods.

Varying Load Power Demand

Finally, simulations were conducted to evaluate the turbine system performance under time-varying load power demand. Load power demand with the form of a sinusoidal function is used as an example to demonstrate the effectiveness of our methodology.

Figure 32 shows the simulation result under real wind speed input and time-varying load power demand which has the following form

$$P_{load}(t) = 15\sin\left(\frac{2\pi}{50}t\right) + 35 \quad \text{kW} \tag{67}$$

From Fig. 32, it is seen that the NOC method still has advantage over the traditional methods in terms of C_p and captured wind power under time-varying load power demand. The load power demand, which is a sinusoidal function, varies between 20 kW and 50 kW with a period of 50 seconds. Due to the variation in the load power demand, switching back and forth between the MISO and the SISO mode frequently happens during turbine's operation. The NOC method is able to maximize the overall wind energy capture throughout turbine's operation by generating the optimal control input trajectories while the traditional methods which are designed for maximizing turbine's efficiency during a specific mode fails to do so.

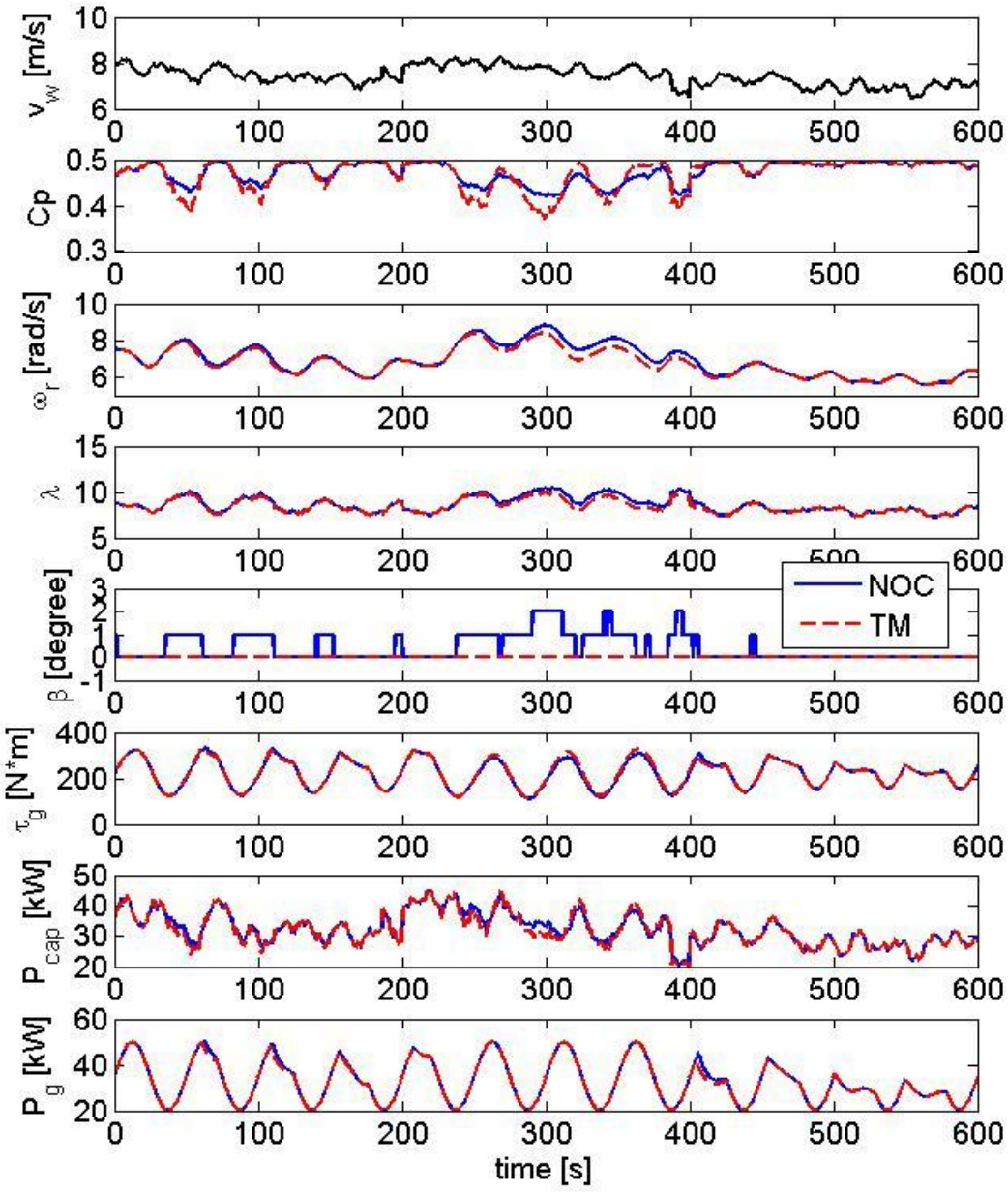

Figure 32: Performance comparison between the NOC method and the traditional methods under real wind speed input and time-varying load power demand.

Table 10 compares the overall wind energy capture for all of the simulation results shown in this section. From the data in Table 10, it is revealed that the NOC method is able to significantly improve the overall wind energy captured by the turbine comparing to that of the traditional methods. The percentage increase in wind energy capture of the NOC method over the TM methods can be up to 29.51%. Even when the load power demand is varying and frequent switching is involved in turbine's operation, the NOC method still enables 0.64% higher wind energy capture compared to the TM methods.

Fig	Wind Profile Duration (seconds)	Wind Energy Capture ($\times 10^3$ kJ)		Percentage Increase over TF (%)
		TM	NOC	
28	80	2.5448	2.5661	0.84
29	80	6.4968	8.3793	29.51
30	600	21.8051	22.1246	1.465
31	600	23.1398	23.3671	0.98
32	600	19.2017	19.3253	0.64

Table 10: A comparison on wind energy capture for all groups of simulations in this chapter.

Chapter 8: *Conclusions and Future Work*

In Chapter 5, an optimal control framework was developed to maximize wind energy capture with reduced computational expense for a speed-constrained wind turbine operating in the partial load region. For this problem, the direct shooting method and dynamic programming algorithm were compared to the traditional method of torque feedback control. It was found that the numerical optimal control method, including DS, DP and ADP, facilitates more wind energy capture than the traditional control, when the turbine speed constraint causes the tip speed ratio to fall in a range where the global maximum of the aerodynamic power coefficient is no longer achievable. In terms of computational expense, to perform as well as the DP and ADP algorithms, the DS method requires additional tuning to find a well-conditioned starting point. The DP method also suffers from excessive computational expense, as it implements an exhaustive search for a global optimal solution. An alternative presented here is the ADP method, which retains the improved energy capture, while avoiding excessive computation. As a result, this research effort establishes an optimal control design framework for maximizing wind energy capture that makes significant improvements towards computational feasibility.

In Chapter 6, the NOC frame work is further enhanced by modifying the performance index to include reducing the turbine generator torque variation. Constant weightings are first incorporated with the modified performance index and the performance of the NOC method using this modified performance index is evaluated by varying the value of the constant weightings. It is found that the NOC method using the modified performance index with constant weightings is able to generate smoother turbine generator torque trajectory and there is a tradeoff between maximizing wind energy capture and the smoothness of the turbine generator torque trajectory. Then, time-varying weightings are

incorporated with the modified performance index to seek further improvement on turbine system performance. By applying time-varying weightings, more wind energy can be captured and smoother generator torque trajectory can be generated compared to that of constant weightings. The approach of adding time-varying weightings is a powerful tool. Varying the form of the weighting functions will provide more leverage in turbine optimal control design.

In Chapter 6, a specific function is picked for the time-varying weighting to demonstrate the effectiveness our methodology. Further experiments can be conducted to test the performance of different functions as the time-varying weightings on turbine systems of different sizes. Furthermore, the approach of the time-varying weightings can also be applied to enhance the performance of the wind turbine system in other aspects, depending on various design requirements. It should also be noted that the wind speed profile used to validate our methodology in this chapter has the form of multiple step inputs, which represents the case in which the wind speed is relative stable and doesn't have large variations within a short time periods. When the wind speed is more volatile, functions with faster decreasing rate need to be used as the time-varying weightings to make the turbine's dynamics react fast enough as the wind speed changes. The simulations results for the system performance under more volatile wind speed input are not shown in this chapter because in that case, the reaction of the turbine becomes much faster and the difference in the smoothness of the generator torque trajectory and the captured wind power becomes less significant. All of the aforementioned topics will be included in our future work.

In Chapter 7, an optimal control framework was developed to maximize the overall wind energy capture of a switched wind turbine system. Through numerical simulations, it was found that the NOC method is able to significantly improve the overall wind energy

capture of the turbine compared to that of the traditional control methods. The traditional methods are designed aiming to maximize turbine's efficiency during a specific operation mode and have been proved to be effective in industry. However, when switching is involved in turbine's operation, applying traditional methods to control turbine's behavior for different modes may not necessarily guarantee the overall maximum wind energy capture. The NOC method, on the other hand, is designed aiming to maximize the overall wind energy of the turbine over the entire time horizon of operation. By generating the optimal control trajectories, the NOC method enables higher wind energy capture than the traditional methods under different wind speed and load conditions. As a result, this research effort establishes an optimal control framework for maximizing the overall wind energy capture of a wind turbine system.

References

[1] The U.S. Department of Energy, 20% Windpower by 2030, United Stated Department of Energy, 2008.

[2] Blanco, M. I., 2009, "The economics of wind energy," Renewable and Sustainable Energy Reviews, 13(6), pp. 1372-1382.

[3] GWEC-Global-Wind-Report 2013.

[4] http://powerturbines.blogspot.com/2014/07/wind-turbine-classifications-basic.html

[5] http://www.wwindea.org/technology/ch01/en/1_2.html

[6] Hall, J. F., 2012, "Design and control of a variable ratio gearbox for distributed wind turbine systems," Dissertation, University of Texas at Austin.

[7] http://www.wind-power-program.com/turbine_characteristics.htm

[8] Pao, L. Y. and Johnson, K. E., 2011, "Control of Wind Turbines," IEEE Control Systems, 31(2), pp. 44-62.

[9] Pao, L. Y. and Johnson, K. E., 2009, "A Tutorial on the Dynamics and Control of Wind Turbines and Wind Farms," American Control Conference, 2009, pp. 2076-2089.

[10] Laks, J. H., Pao, L. Y. and Wright, A. D., 2009, "Control of Wind Turbines: Past, Present, and Future," American Control Conference, 2009, pp. 2096 - 2103.

[11] Johnson, K. E., Fingersh, L. J., Balas, M. J. and Pao, L. Y., 2004, "Methods for Increasing Region 2 Power Capture on a Variable-Speed Wind Turbine," Journal of Solar Energy Engineering, 126(4), pp. 1092-1100.

[12] Wright, A. K. and Wood, D. H., 2007, "Yaw Rate, Rotor Speed and Gyroscopic Loads on a Small Horizontal Axis Wind Turbine, " Wind Engineering, 31(3), pp. 197-209.

[13] Muljadi, E. and Butterfield, C. P., 2001, "Pitch-controlled variable-speed wind turbine generation, " IEEE Transactions on Industry Applications, 37(1), pp. 240-246.

[14] Hinrichsen, E. N., 1984, "Controls for Variable Pitch Wind Turbine Generators," IEEE Transactions on Power Apparatus and Systems, 4(4), pp. 44-45.

[15] Heier, S., 2006, Grid integration of wind energy conversion

systems, 2nd ed., Wiley, New York, NY.

[16] Hall, J. F., Mecklenborg, C. A., Chen, D., and Pratap, S. B., 2011, "Wind energy conversion with a variableratio gearbox: design and analysis," Renewable Energy, 36(3), pp. 1075-1080.

[17] Hand, M. M. and Balas, M. J., 2000, "Systematic controller design methodology for variable-speed wind turbines, " Wind Energy, 24(3), pp. 169-187.

[18] Koutroulis, E. and Kalaitzakis, K., 2006, "Design of a maximum power tracking system for wind energyconversion applications," IEEE Transactions on Industrial Electronics, 53(2), pp. 486-494.

[19] Wang, Q. C. and Chang, L. C., 2004, "An intelligent maximum power extraction

algorithm for inverter-based variable speed wind turbine systems," IEEE Transactions on Power Electronics, 19(5), pp. 1242-1249.
[20] Barakati, S. M., Kazerani, M. and Aplevich, J. D., 2009, "Maximum Power Tracking Control for a Wind Turbine System Including a Matrix Converter," IEEE Transactions on Energy Conversion, 24(3), pp. 705-713.
[21] Dalala, Z. M., Zahid, Z. U., Yu,W., Cho, Y. and Lai, J., 2013, "Design and Analysis of an MPPT Technique for Small-Scale Wind Energy Conversion Systems," IEEE Transactions on Energy Conversion, 28(3), pp. 756-767.
[22] Petrila, D. , Blaabjerg, F. , Muntean, N. and Lascu, C., 2012 "Fuzzy logic based MPPT controller for a small wind turbine system," Optimization of Electrical and Electronic Equipment (OPTIM), 2012 13th. International Conference, 2012, pp. 993-999.
[23] Soetedjo, A., Lomi, A. and Mulayanto, P., 2011, "Modeling of Wind Energy System with MPPT Control," Proceedings of the 2011 International Conference on Electrical Engineering and Informatics, 2011, pp. 1-6.
[24] Beltran, B., Ahmed-ali, T., and Benbouzid, M., 2009, "High Order Sliding Mode Control of Variable-Speed Wind Turbines, " IEEE Transactions on Industrial Electronics, 56(9), pp. 3314-3321.
[25] Barambones, O., 2012, "Sliding Mode Control Strategy for Wind Turbine Power Maximization, " Energies, 5(12), pp. 2310-2330.
[26] Schlipf, D. and Cheng P. W., 2013, "Adaptive Feed Forward Control for Wind Turbines," ATAUTOMATISIERUNGSTECHNIK, 61(5), pp. 329-338.
[27] Johnson, K. E., Pao. L. Y., Balas, M. J. and Fingersh, L. J., 2006, "Control of variable-speed wind turbines: standard and adaptive techniques for maximizing energy capture," IEEE Control Systems, 26(3), pp. 70-81.
[28] Song, Y. D., Dhinakaran, B. and Bao, X. Y., 2000, "Variable speed control of wind turbines using nonlinear and adaptive algorithms," Journal of Wind Engineering & Industrial Aerodynamics, 85(3), pp. 293-308.
[29] Frost, S. A., Balas, M. J. and Wright, A. D., 2009, "Direct adaptive control of a utility-scale wind turbine for speed regulation," International Journal of Robust and Nonlinear Control, 19(1), pp. 59-71.
[30] Johnson, K. E., 2004, "Adaptive torque control of variable speed wind turbines," NREL/TP-500-36265.
[31] Bianchi, F. D., Mantz, R. J. and Christiansen, C. F., 2004, "Control of variable-speed wind turbines by LPV gain scheduling, " Wind Energy, 7(1), pp. 1-8.
[32] Venne, P., Guilaud, X., Teodorescu, R. and Mahseredijian, J., 2010, "Generalized Gain Scheduling for Deloaded Wind Turbine Operaiton, " Wind Engineering, 34(2), pp. 219-240.
[33] Hammerum, K., Brath, P. and Poulsen, N. K. 2007, "A fatigue approach to wind turbine control," Journal of Physics, 75, pp. 123081.
[34] Palejiya, D., Hall, J., Mecklenborg, C. and Chen, D., 2013, "Stability of Wind Turbine Switching Control in an Integrated Wind Turbine and Rechargeable Battery System: A Common Quadratic Lyapunov Function Approach, " Journal of Dynamic Systems

Measurement and Control-Transactions of the ASME, 135(2), pp. 021018(1-9).

[35] Shorten, R., Wirth, F., Mason, O., Wulff, K., and King, C., 2007, "Stability Criteria for Switched and Hybrid Systems, " SIAM Review, 49(4), pp. 545-592 .

[36] Liberzon, D. and Morse, A. S., 1999, "Basic Problems in Stability And Design of Switched Systems," IEEE Control Systems Magazine, 19, pp. 5970.

[37] Chesi1, G., Colaneri, P., Geromel, J. C., Middleton, R., Shorten, R., "Computing Upper-Bounds of The Minimum Dwell Time of Linear Switched Systems Via Homogeneous Polynomial Lyapunov Functions," In Proceedings of 2010 American Control Conference, 2010

[38] Wicks, M. A., Peleties, P., and DeCarlo, R., "Construction of Piecewise Lyapunov Functions for Stabilising Switched Systems," In Proceedings of the 33rd Conference on Decision and Control, Lake Buena Vista, FL, 1994, pp. 34923497.

[39] Zhai, G., Hu, B., Yasuda, K. and Michel, A.N., 2001, "Stability Analysis of Switched Systems with Stable And Unstable Subsystems: An Average Dwell Time Approach," International Journal of Systems Science, 32(8), pp. 1055 - 1061.

[40] Chase, C., Serrano, J., and Ramadge, P., 1993, "Periodicity and Chaos from Switched Flow Systems: Contrasting Examples of Discretely Controlled Continuous Systems," IEEE Trans. Automat. Control, vol. 38, pp. 7083.

[41] Zhao, J. and Hill D., 2008, "On Stability, L2 gain and H1 control for switched systems," Automatica, 44(5), pp 1220-1232.

[42] Sebe, N. and Suyama, K., 2011, "L2 gain analysis of linear systems with a single switching," International Journal of Robust and Nonlinear Control, 21(8), pp. 827 – 837.

[43] Fang, H., Liu, Z., and Lu, L., 2009, "L2 gain analysis for a class of switched systems," Automatica, 45(4).

[44] Hespanha, J., 2004, "Stochastic Hybrid Systems: Application to Communication Network, in Hybrid Systems: Computation And Control," Proceedings of the 7th International Workshop, HSCC 2004, Philadelphia, PA, Springer, Berlin, 2004, pp. 387–401.

[45] Morroni, J., Corradini, L., Zane, R., and Maksimovic, D., 2009, "Robust Adaptive Tuning of Digitally Controlled Switched-Mode Power Supplies," in Proc. IEEE Appl. Power Electron. Conf. Expo., Washington, DC, Feb. 2009, pp. 240-246.

[46] Buntin, D. L. and Howze, J. W., 1995, "Switching Logic Controller for A Hybrid Electric/ICE Vehicle," In Proceedings of American Control Conference. 1995.

[47] Wulff, K., Foy, J. and Shorten, R., 2003, "Comments on Periodic and Absolute Stability for Switched Linear Systems", in Proceedings of the American Control Conference, Denver, CO, 2003.

[48] Lin, H. and Antsaklis, P. J., 2005, "Stability and Stabilizability of Switched Linear Systems: A Short Survey of Recent Results," Proceedings of the 2005 IEEE International Symposium on Intelligent Control, Limassol, Cyprus, June 27-29, 2005.

[49] Liberzon, D. and Morse, A. S., 1999, "Basic Problems in Stability and Design of Switched Systems," IEEE Control Systems Magazine, 19(5), pp. 59-70.

[50] DeCarlo, R., Branicky, M., Pettersson, S. and Lennartson, B., 2000, "Perspectives And Results On The Stability And Stabilisability of Hybrid Systems," Proc. IEEE, vol. 88, pp. 1069–1082.

[51] Michel, A., 1998, "Recent Trends in the Stability Analysis of Hybrid Dynamical Systems," IEEE Trans. Circuits and Systems, 45, pp. 120–133.

[52] Akermann, T., 2005, Wind Power in Power Systems, Wiley, New York, NY.

[53] Carlin, P. W., Laxson, A. S. and Muljadi, E. B., 2003, "The History and State of the Art of Variable Speed Wind Turbine Technology," Wind Energy, 6(2), pp. 129-159.

[54] Hall, J. F. and Chen, D., 2012 "Performance of a 100 kW Wind Turbine with a Variable Ratio Gearbox," Renewable Energy, 44, pp. 261-266.

[55] Schlipf, D., Schlipf, D. J. and Kuhn, M., 2013,"Nonlinear model predictive control of wind turbines using LIDAR," Wind Energy, 16(7), pp. 1107-1129.

[56] Liu, J. and Peng, H., 2008, "Modeling and Control of a Power-Split Hybrid Vehicle," IEEE Transactions on Control Systems Technology, 16(6), pp. 1242-1251.

[57] Stryk, O. and Bulirsch, R., 1992, "Direct and indirect methods for trajectory optimization," Annals of Operations Research, 37(1), pp. 357-373.

[58] Hull, D. G., 2003, Optimal Control Theory for Applications, Springer, New York, NY.

[59] Sargent, R. W. H., 2000, "Optimal Control," Journal of Computational and Applied Mathematics, 124(1), pp. 361-371.

[60] Hull, D. G., 1997, "Conversion of Optimal Control Problems into Parameter Optimization Problems," Journal of Guidance Control and Dynamics, 20(1), pp. 57-60.

[61] Gornov, A. Y., Tyatyushkin, A. I. and Finkelstein, E. A., 2013, "Numerical methods for solving applied optimal control problems," Computational Mathematics and Mathematical Physics, 53(12), pp. 1825-1838.

[62] Noton, A., Dyer, P. and Markland, C., 1967, "Numerical computation of optimal control," IEEE Transactions on Automatic Control, 12(1), pp. 59 - 66.

[63] Bryson, A.E. and Ho, Y-C, "Applied optimal control," Rev. Printing, Hemisphere, New York, 1975.

[64] Hestenes, M.R., "Calculus of the variations and optimal control theory," Wiley, 1966.

[65] Kirk, D.E., "Optimal Control Theory: An Introduction", Englewood Cliffs, N.J.: Prentice-Hall, 1970.

[66] Betts, J. T., 1998, "Survey of Numerical Methods for Trajectory Optimization," Journal Of Guidance, Control, And Dynamics, 21(2), pp.193-207.

[67] Błaszczyk, J., Karbowski, A., and Malinowski, K., 2007, "Object Library Of Algorithms For Dynamic Optimization Problems: Benchmarking Sqp And Nonlinear Interior Point Methods," Int. J. Appl. Math. Comput. Sci., 17(4), pp. 515–537.

[68] Lewis, F.L. and Syrmos, V.L., "Optimal Control", John Wiley & Sons, Inc., 1995

[69] Hager, W. W., 1999, "Stabilized Sequential Quadratic Programming," Computational Optimization and Applications, 12(1), pp. 253-273.

[70] Frank, E. C. and Michael, L. O., 2012, "A Sequential Quadratic Programming Algorithm for Nonconvex, Nonsmooth Constrained Optimization," SIAM Journal on Optimization, 22(2), pp. 474-500.
[71] Paul T. Boggs and Jon W. Tolle, 1995, "Sequential Quadratic Programming," Acta Numerica, 4, pp. 1-51.
[72] Nocedal, J. and Wright, S. J., 2006, "Numerical Optimization," Second Edition, Springer Series in Operations Research and Financial Engineering, ISBN 0387303030.
[73] Bartholomew–Biggs, Michael, 2008, "Nonlinear Optimization with Engineering Applications," Springer Optimization and Its Applications, 19, pp. 1 – 14.
[74] Bertsekas, D. P., "Nonlinear programming," 2003, 2nd ed., 2nd printing [rev.], ISBN 1886529140.
[75] Bazaraa, Mokhtar S; Sherali, Hanif D; Shetty, C. M, "Nonlinear Programming: Theory and Algorithms," 2006, 3. Aufl., ISBN 9780471486008
[76] Luenberger, David G., 1937 and Ye, Yinyu, "Linear and nonlinear programming," 2008, Third Edition, International series in operations research & management science, ISBN9780387745022.
[77] Sun, Wenyu and Yuan, Ya-xiang, "Optimization theory and methods: nonlinear programming," 2006, Springer optimization and its applications, ISBN 9780387249759.
[78] Peressini, Anthony L; Sullivan, Francis E; Uhl, J. J. (J. Jerry), "The mathematics of nonlinear programming," 1988, Undergraduate texts in mathematics, ISBN 9780387966144.
[79] Wang, F., Zhang, H. and Liu, D., 2009, "Adaptive Dynamic Programming: An Introduction," IEEE Computational Intelligence Magazine, 4(2), pp. 39-47.
[80] Iyengar, G. N., 2005, "Robust Dynamic Programming," Mathematics of Operations Research, 30(2), pp. 257-280.
[81] Sniedovich, Moshe, "Dynamic programming: foundations and principles," 2010, 2nd ed., Monographs and textbooks in pure and applied mathematics, ISBN 9780824740993.
[82] Zabczyk, Jerzy, "Mathematical Control Theory," 2008, Modern Birkhäuser Classics, ISBN 0817647325.
[83] Bertsekas, D. P, "Dynamic programming and optimal control," 1995, ISBN 9781886529120.
[84] Rajagopalan, A. and Hariharan, M. V., 1974, "Bang-Bang Excitation Control," IEEE Transactions on Power Apparatus and Systems, PAS-93(2), pp. 703-711.
[85] Walsh, G. R., 1972, "A numerical example of optimal bang-bang controls," Journal of Engineering Mathematics, 6(2), pp. 165-174.
[86] Thompson, W. and Jain, V., 1966, "Bang-bang parameter optimization," IEEE Transactions on Automatic Control, 11(3), pp. 615-616.
[87] Wait, T. R., 2012, "Turbine-generator shaft torsional vibrations resulting from transmission line transients," Power and Energy Society General Meeting, 2012, pp.

1-4.
[88] Y, Xu. and R, He., 2006, "Analysis of the Failure in a Turbine-Generator Shaft," International Conference on Power System Technology, 2006, pp. 1-6.
[89] Wang, Z., Shen, J., Rowan, B. and Hingwe, P., 2010, "Optimal seek profile generation with time-varying weightings for hard disk drives," Microsystem Technologies, 16(1-2), pp. 111-115.
[90] De la Cruz, H., Biscay, R. J., Jimenez, J. C. and Carbonell, F., 2013, "Local Linearization -- Runge-Kutta methods: A class of A-stable explicit integrators for dynamical systems," Mathematical and Computer Modeling, 57(3-4), pp. 720.
[91] Udwadia, F. E. and Farahani, A., 2008, "Accelerated Runge-Kutta Methods," Discrete Dynamics in Nature and Society, 14(2), pp. 1 – 38.
[92] Dormand J. R. and Prince, P. J., 1989, "Practical Runge-Kutta Processes," Society for Industrial and Applied Mathematics. SIAM Journal on Scientific and Statistical Computing, 10(5), pp. 977.
[93] National Renewable Energy Laboratory (NREL), from http://www.nrel.gov/
[94] Lexa, M. A., Davies, M. E., Thompson, J. S. and Nikolic. J., 2011, "Compressive power spectral density estimation," IEEE International Conference on Acoustics, Speech, and Signal Processing (ICASSP), 2011, pp. 3884-3887.
[95] Lee, D. and Baldick, R., 2013, "Future Wind Power Scenario Synthesis Through Power Spectral Density Analysis," IEEE Transactions on Smart Grid, 5(1), pp. 490-500.
[96] The Wind Power Program, from http://www.windpower- program.com